

T-1684

LIQUID LITHIUM CORROSION OF
TYPE 304L STAINLESS STEEL

By

Richard Alan Patterson

ProQuest Number: 10781931

All rights reserved

INFORMATION TO ALL USERS

The quality of this reproduction is dependent upon the quality of the copy submitted.

In the unlikely event that the author did not send a complete manuscript and there are missing pages, these will be noted. Also, if material had to be removed, a note will indicate the deletion.



ProQuest 10781931

Published by ProQuest LLC (2018). Copyright of the Dissertation is held by the Author.

All rights reserved.

This work is protected against unauthorized copying under Title 17, United States Code
Microform Edition © ProQuest LLC.

ProQuest LLC.
789 East Eisenhower Parkway
P.O. Box 1346
Ann Arbor, MI 48106 – 1346

SUBMITTAL SHEET

A Thesis submitted to the Faculty and the Board of Trustees of the Colorado School of Mines in partial fulfillment of the requirements for the degree of Masters of Science, Metallurgical Engineering.

Signed: *R. Patterson*
Student

Golden, Colorado

Date: *Aug. 28, 1974*

Approved: *David Z. Olson*
Thesis Advisor

R. J. [Signature]
Head of Department

Golden, Colorado

Date: *Aug 28, 1974*

JOHN LAKES LIBRARY
COLORADO SCHOOL OF MINES
GOLDEN, COLORADO

ABSTRACT

The measurements of the depth of penetration and weight loss per unit surface area are used to explain the corrosion behavior of 304L stainless steel in liquid lithium. Of these measurements the depth of penetration is the most reliable due to the non-uniform nature of the corrosion attack.

The grain boundary penetration was found to follow a parabolic time dependence. Also the delay time for the initiation of penetration process was explained by the incubation time necessary to nucleate a (Li-Me-N) complex. Thus the advancement of the penetration was suggested to be controlled by the diffusion of either lithium or nitrogen down the (Li-Me-N) complex compound-austenitic grain boundary interface.

The weight loss was found to be dependent upon an initial uniform dissolution of alloying constituents and followed by a non-uniform deterioration of the surface. The initial weight loss behavior was also found to be thermally activated.

The corrosion of 304L stainless steel in liquid lithium was found to be strongly dependent on the concentration of impurities. The corrosion rate for both penetration and weight loss were shown to be dependent upon the nitrogen concentration of the lithium. The titanium gettering of the nitrogen from the lithium was found to reduce both the rate of penetration and the amount of weight lost per unit surface area.

TABLE OF CONTENTS

	<u>Page</u>
INTRODUCTION	1
Liquid Lithium Characteristics	2
Review of Compatibility Work	4
Dissolution	4
Dissimilar Metals	10
Impurity Effects	12
Investigation	18
EXPERIMENTAL PROCEDURE	19
Materials	19
Apparatus	21
Testing	24
Metallography	26
RESULTS	31
Grain Boundary Penetration	33
Titanium Gettering	37
Reliability of Data	40
Dissolution and Surface Deterioration	40
Impurity Effects	49
Titanium Gettering	49
Nitric Acid Contamination	52

	<u>Page</u>
DISCUSSION OF RESULTS	56
Delay Time	57
Grain Boundary Penetration	57
Impurity Effects	64
CONCLUSION	67
SUGGESTIONS FOR FURTHER RESEARCH	68
APPENDIX I	69
REFERENCES	75

LIST OF FIGURES

ARTHUR LAKES LIBRARY
 COLORADO SCHOOL OF MINES
 GOLDEN, COLORADO

<u>Figure</u>	<u>Page</u>
1. Typical qualitative evaluation of materials in liquid lithium - After Lyons ⁽¹⁸⁾ .	5
2. Solubilities of Ni, Cr, Fe, Ti, and Mo in liquid lithium.	7
3. Schematic diagram of a heat exchanger loop.	9
4. Schematic diagram explaining dissimilar metal effects.	11
5. Nitrogen effects on the solubilities of titanium and niobium in liquid lithium.	13
6. Free energies of formation of oxides, carbides hydrides, nitrides, sulfides and silicides.	17
7. Li ₃ N portion of the Li-N phase diagram.	22
8. Schematic diagram of the test crucible.	23
9. Micrograph showing the as heat treated 304L stainless steel.	26
10. Micrographs comparing the penetration zones as revealed by metallography.	30
11. Penetration depth versus the square root of time for 600, 650, 727, and 800 C.	34
12. Penetration depth versus the square root of time for 800, 900, 1000 C.	35
13. Temperature dependence of the delay time.	36

<u>Figure</u>	<u>Page</u>
14. Arrhenius plot for grain boundary penetration.	38
15. Comparison of the grain boundary penetration for the nitrogen saturated lithium and the titanium gettered lithium.	41
16. Weight loss per unit surface area versus the square root of time at 600 C.	42
17. Weight loss per unit surface area versus the square root of time at 650 C.	43
18. Weight loss per unit surface area versus the square root of time at 727 C.	44
19. Weight loss per unit surface area versus the square root of time at 800 C.	45
20. Weight loss per unit surface area versus the square root of time at 900 C.	46
21. Arrhenius plot for the initial weight loss behavior.	48
22. Weight loss per unit surface area versus the square root of time for the titanium gettered lithium.	51
23. Typical micrograph of the uniform corrosion scale created on the nitric acid contaminated corrosion samples.	53
24. Comparison of weight loss behavior for the methanol cleaned and the nitric acid contaminated corrosion samples.	54

<u>Figure</u>	<u>Page</u>
25. Arrhenius plot showing the proposed rate controlling species for the grain boundary penetration.	59
26. Schematic diagrams for the grain boundary penetration model.	61
27. Nitrogen effects on the grain boundary penetration behavior.	65

LIST OF TABLES

<u>Table</u>	<u>Page</u>
1. Neutron-absorption cross sections.	3
2. Possible liquid metal-containment metal interactions.	6
3. Li_3N effects on the corrosion of type 316 stainless steel in liquid lithium.	14
4. Chemical analysis of type 304L stainless steel.	20
5. Matrix of tests performed.	25
6. Chemical etches and procedures used for metallography.	29
7. Grain boundary penetration rate coefficients.	39
8. Activation energies for grain boundary penetration.	39
9. Rate coefficients and activation energy for the weight loss study.	50

ACKNOWLEDGEMENTS

The author gratefully appreciates the expert guidance and advice provide by his thesis advisor, Dr. D. L. Olson, and the thesis committee, Dr. W. L. Bradley and Dr. D. K. Matlock. Also an expression of kind thanks to Dr. A. W. Schlechten, who substituted for Dr. Bradley during the thesis defense.

Financial support for this investigation was provided by the Atomic Energy Commission.

Finally an expression of sincere gratitude is extended to my loving wife Pam and my son Brian, without whom this work would be incomplete and meaningless.

INTRODUCTION

With the oncoming implementation of nuclear power generation, there will be a need for an efficient and safe high-temperature heat transfer medium. To date, liquid sodium and liquid sodium-potassium alloys⁽¹⁻¹¹⁾ have been subjected to many laboratory and in-practice investigations to determine the feasibility of containing these metals in coolant systems for the Liquid Metal Fast Breeder Reactor (LMFBR). Liquid lithium⁽¹²⁻²⁰⁾ is also being considered for use as a coolant medium due to its superior physical properties.

The major problem in the use of liquid metals as coolant mediums is their reactive nature when coupled with the common construction materials. From the past liquid sodium work⁽¹⁻¹¹⁾, this compatibility problem has been related to a uniform dissolution attack and an accelerated grain boundary attack, both of which are interrelated with other operating variables, i.e. impurity concentrations, dissimilar metal effects, and non-isothermal flowing-liquid systems. The investigation reported in this thesis is concerned with the nature of liquid lithium corrosion on austenitic stainless steel. From this study, correlations are made which allow a better understanding of the controlling mechanisms.

Liquid Lithium Characteristics

Interest in alkali metals has increased recently due to the need of an efficient coolant for the Liquid Metal Fast Breeder Reactor (LMFBR) and the proposed fusion reactor. The physical characteristics of liquid lithium are well suited for coolant systems in which large temperature ranges and long service life are important. These characteristics include the lowest specific gravity (0.5 gm/cm^2), a low melting temperature (186 C), a large molten range (186 - 1337 C), the highest specific heat (0.70 cal/g), the highest heat of fusion (159 cal/g) and the highest heat of combustion of the low melting metals. (15,21,22)

A low neutron-absorption cross section for the liquid metal coolant is also important for an efficient thermal reactor. (25) Table 1 shows a comparison of the neutron cross sections of the possible coolant mediums. (23-25) From Table 1 it can be seen that Lithium-7 also has the lowest neutron absorption cross section of any of these candidates for coolants. Another advantage to Lithium-7 is that, upon neutron capture, it becomes Lithium-8 which has a very short half life of approximately .85 seconds and emits only a weak beta radiation. Thus liquid lithium would lose any radioactivity quickly and the primary heat exchanger of the nuclear reactor could be placed exterior to the major radiation shielding. With the primary heat exchanger placed exterior to the radiation shielding, system inspection and repair is made much easier.

TABLE I (25)

NEUTRON-ABSORPTION CROSS SECTIONS

Liquid Metal	Macroscopic at 343 C, cm^{-1}	Barns, $\text{cm}^2 \times 10^{-24}$
Na-23.....	0.0074	0.45
K.....	0.0166	2.5
Li-6.....		984.0
Li-7.....	0.00097	0.033
B1-209.....	0.00059	0.03
^{56}Na - ^{44}K	0.0113	1.1
97.5Pb-2.5Mg.....	0.0040	0.21
55.5B1-44.5Pb.....	0.0021	0.17

Review of Compatibility Work

The initial efforts to study the containment of liquid metals were concerned with a qualitative screening of the potential container materials. Figure 1 shows a typical report of materials qualitatively categorized as to their resistance to a corrosive attack by liquid lithium. Possible container materials could be selected from a report similar to that shown in Figure 1, then subjected to a more rigorous examination of their corrosion rates in liquid metals.

A quantitative investigation of corrosion rates must include a study of the many possible interactions encountered in a coolant system for high temperature applications. Table 2 shows a list of these possible interactions between containment metals and liquid metal coolants. The following review of research, performed with respect to each of these interactions, will clarify the problem of containing liquid metals at the temperatures necessary for nuclear applications.

Dissolution

The chemical equilibrium between the containment metal or its alloy constituents and the liquid metal is the driving force for a dissolution process.⁽¹⁰⁾ This chemical equilibrium is defined by the solubility of the containment metal species in the liquid metal. Figure 2⁽²⁶⁾ shows the solubilities of the major constituents of austenitic stainless steels in liquid lithium. As can be seen from Figure 2, low

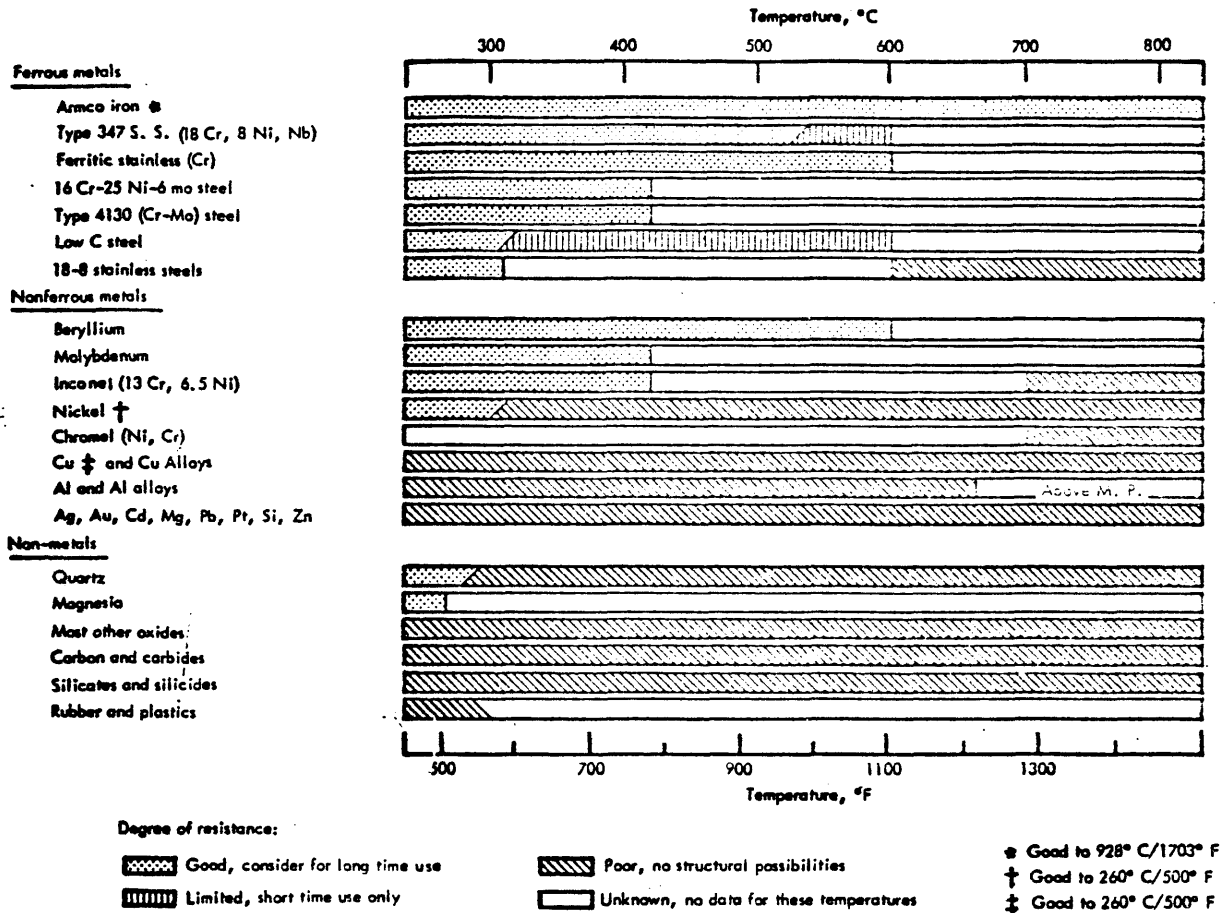


Figure 1. A listing of materials investigated for possible applications in lithium and a qualitative evaluation of their resistance to a corrosive attack by lithium. From Lyons⁽¹⁸⁾.

ARTHUR LAKES LIBRARY
 COLORADO SCHOOL OF MINES
 GOLDEN, COLORADO

TABLE 2

TYPES OF INTERACTIONS OF CONCERN TO LIQUID METAL CORROSION

1. Dissolution - Deposition

- a. Isothermal solubility
- b. Temperature gradient mass transfer
- c. Concentration gradient mass transfer

2. Complex Compound Formation

- a. Impurity effects
- b. Gettering

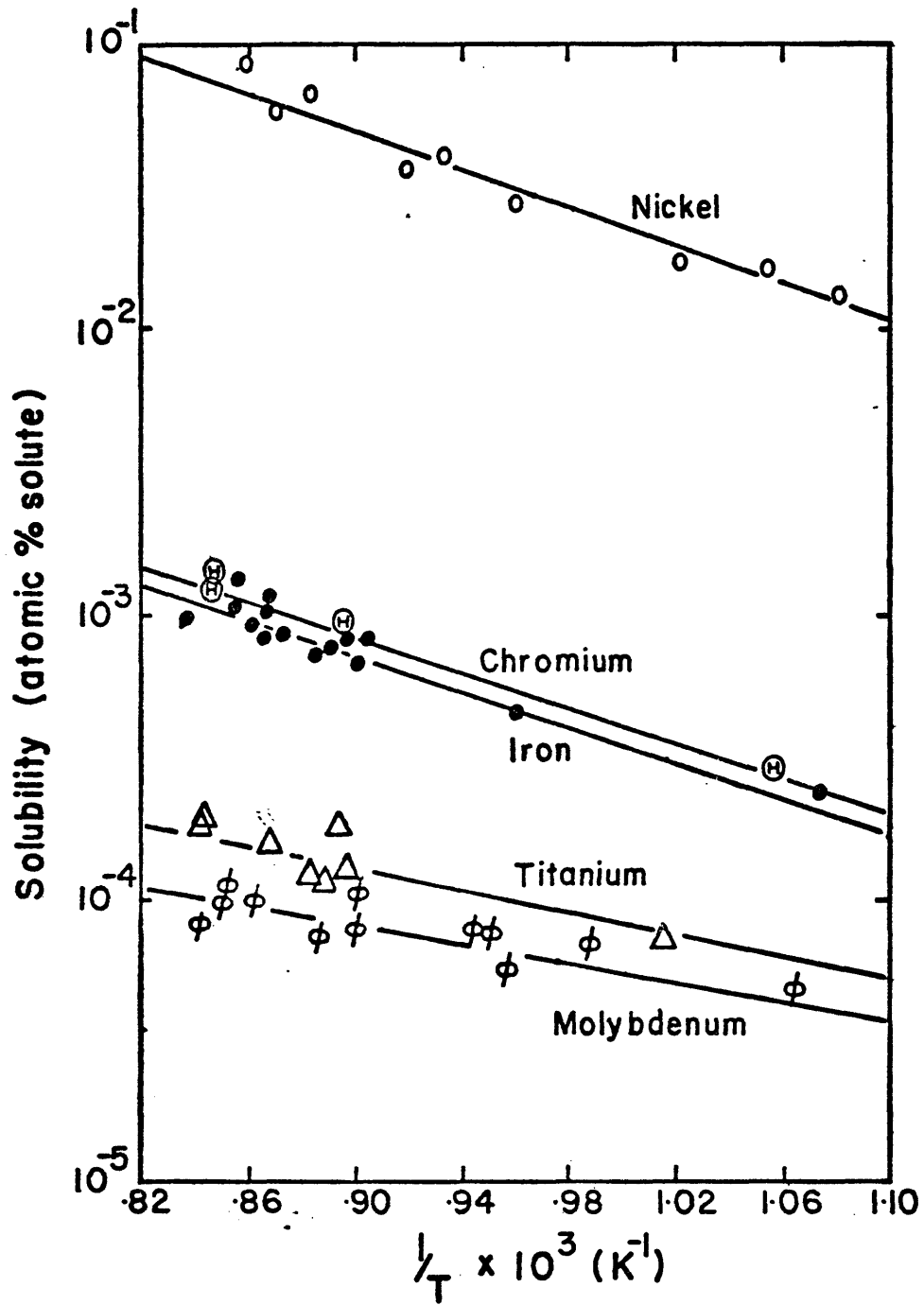


Figure 2. The temperature dependence of the solubilities of a number of metals. Data taken from Leavenworth and Cleary.(26)

concentrations of solute dissolved in the liquid lithium satisfy the solubility limit.

An important factor in the dissolution process is that alloying constituents should be preferentially dissolved according to their individual solubilities. In other words, nickel should be dissolved from austenitic stainless steels in liquid lithium to a greater degree than is either iron or chrome (Figure 2). This is in fact the physical situation as confirmed by chemical analysis of lithium corroded austenitic stainless steels.^(5,8,12) Brasunas⁽²⁷⁾ found that since nickel is preferentially leached from austenitic stainless steels, a surface layer of material transforms to ferrite which could change the corrosion behavior of these metals. However, this observation was only made at high temperatures (1000 C) and after long times (400 hrs), which eliminates the major importance of any surface transformations at the practical application temperatures (600 C).

Many investigators^(1-10,12,13) have reported an increase in the apparent uniform corrosion rate of containment metals and alloys when subjected to flowing liquid metals in non-isothermal systems. Figure 3 illustrates the concept of a heat exchanger loop in which a constant dissolution-deposition process is established. The liquid metal would leach out soluble container elements at the high temperature region in an attempt to achieve chemical equilibrium, then deposit these

TEMPERATURE GRADIENT MASS TRANSFER

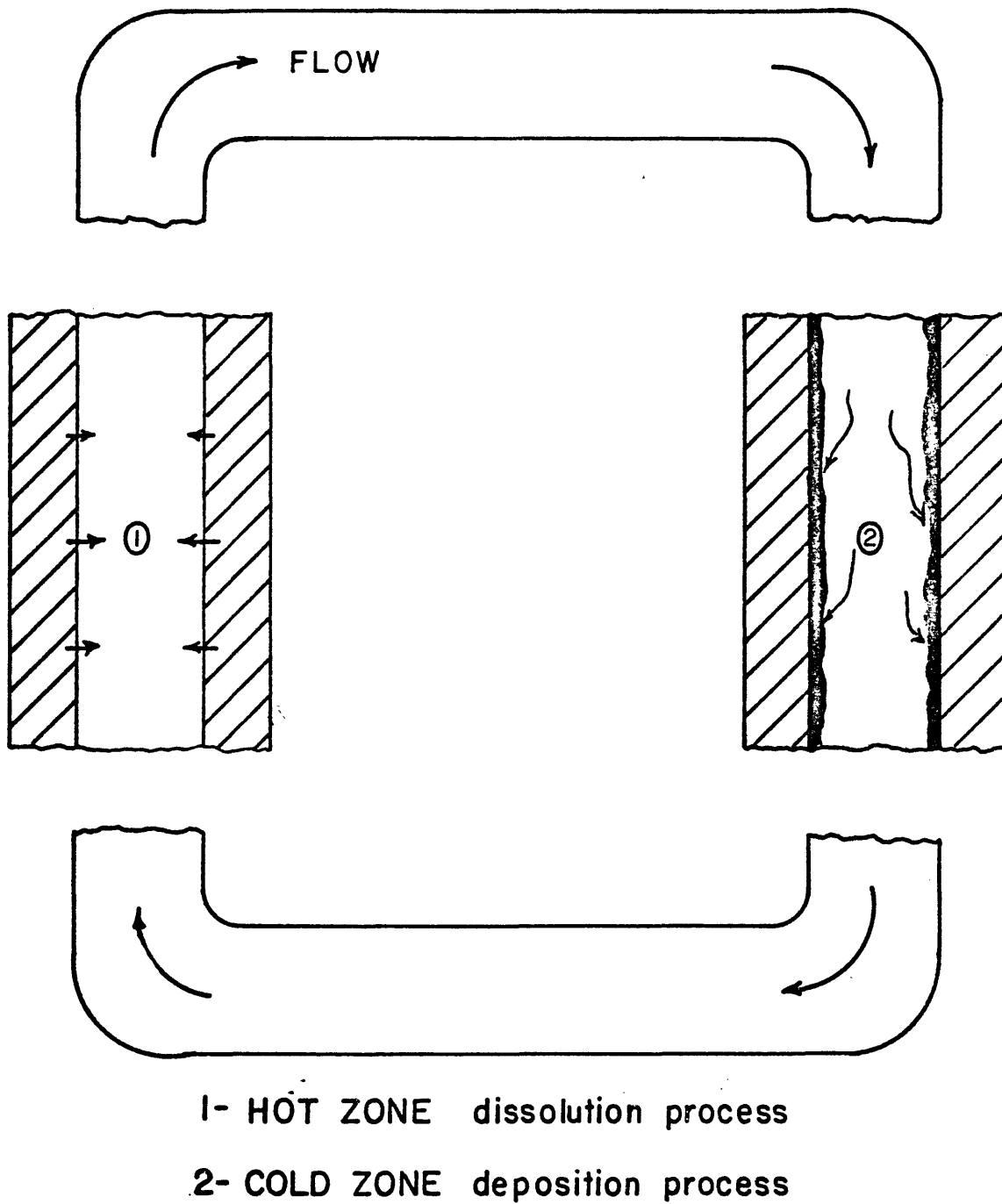


Figure 3. A schematic diagram of the concept of a loop containing flowing liquid metal in the presence of temperature gradients.

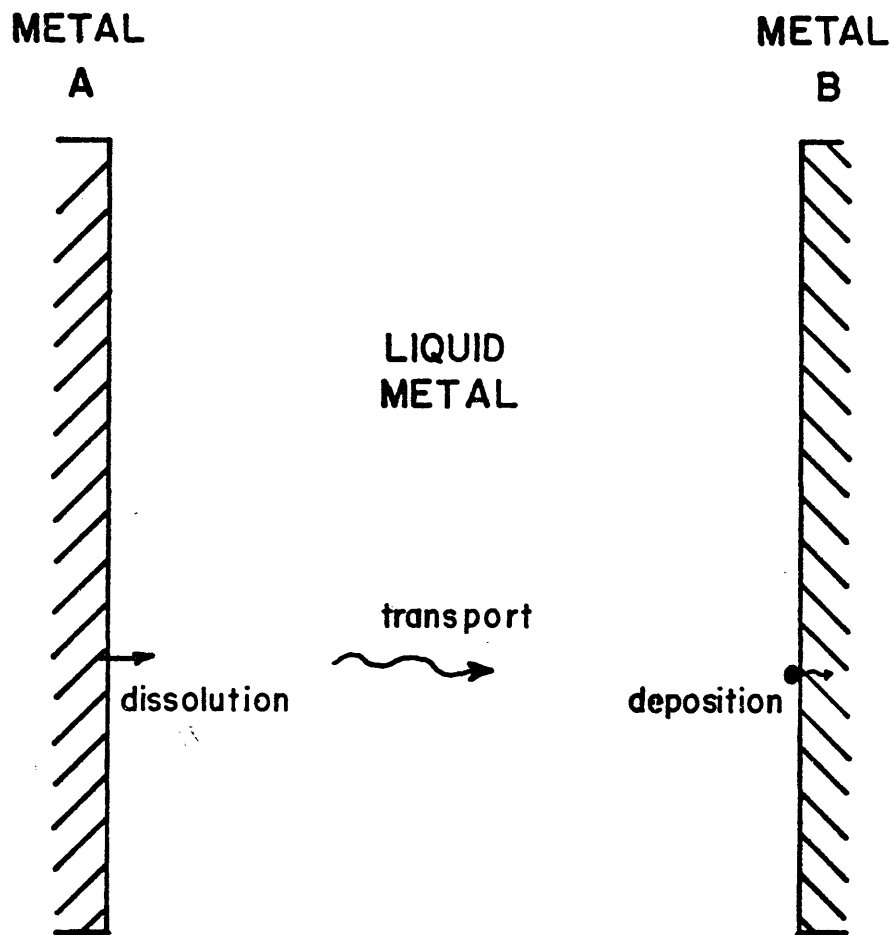
elements at the low temperature region due to the decrease in solubility with decreasing temperatures.

This dissolution-deposition process has been determined^(5,8) to be controlled by the rate of deposition in the low temperature region of the heat exchanger loop. Therefore the failure of such a coolant system would be due to the constriction caused when the deposits begin to gap the piping system as was observed by many investigators.^(5,12,13)

Dissimilar Metals

A second dissolution-deposition process has been found⁽²⁷⁻³²⁾ to be maintained by the use of dissimilar metals in the same containment system. Figure 4 illustrates the mass transport process formed when the dissimilar metals A and B are mutually in contact with a liquid metal. This type of mass transport system can be caused⁽²⁸⁻³³⁾ by alloy concentration variations or by the presence of two different pure metals of which one is soluble in the other.

Examples of dissimilar metal mass transport systems range from carbon transport^(29,31,32), due to the use of two different grades of steel, to transport caused by the segregation of interstitials⁽³⁴⁾ when metals are welded. Hoffman⁽²⁸⁾ has also reported the transport of pure nickel through liquid sodium to deposit on pure molybdenum. Another example of dissimilar metal mass transport is the transport of vanadium from vanadium alloys to a type 321 stainless steel, as was found by Romano, et. al.⁽³⁰⁾



DISSIMILAR METAL EFFECTS

Figure 4. A schematic diagram showing the mass transport possible in the presence of dissimilar metals or concentration gradients.

Klueh⁽⁴⁰⁾ determined that dissimilar metal mass transfer increases with increasing temperature, exposure time and impurity concentration of liquid lithium. Since the high temperature regions of a nuclear reactor must be designed for long time usage, care must be taken to minimize the interaction of dissimilar metals or concentration gradients in this region.

Impurity Effects

The presence of oxygen, nitrogen, and carbon impurities in corrosion systems has been found⁽³⁵⁻³⁷⁾ to accelerate the rate of a liquid metal attack on containment metals. Figures 5a and 5b⁽²⁶⁾ show that an increase in the solubility of both titanium and niobium in liquid lithium is evidenced when the nitrogen concentration of the lithium is increased. Table 3⁽⁴⁶⁾ also indicates that additions of Li_3N to liquid lithium increases the rate of weight loss and grain boundary penetration of type 316 stainless steel. The increased solubility and grain boundary penetration, with increasing impurity concentration, implies that some sort of lithium-containment metal-impurity reaction is responsible for the corrosion behavior.

Klueh⁽⁴⁰⁾ determined that a "threshold" concentration of oxygen was necessary to initiate the grain boundary penetration of niobium by oxygen contaminated lithium. Using the concept of this "threshold" level of oxygen, Brehm⁽³⁵⁾ postulated the formation of a (Nb-O-Li) complex corrosion product in the grain boundaries of his niobium samples. Klueh⁽⁴⁷⁾ also suggested

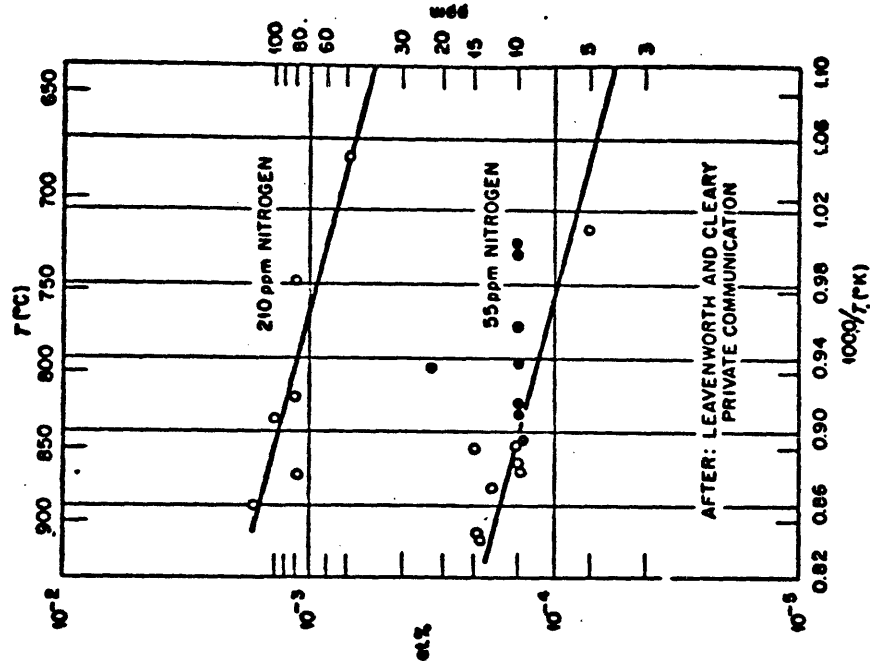


Figure 5b. The solubility of titanium as a function of the temperature and the nitrogen concentration of liquid lithium.

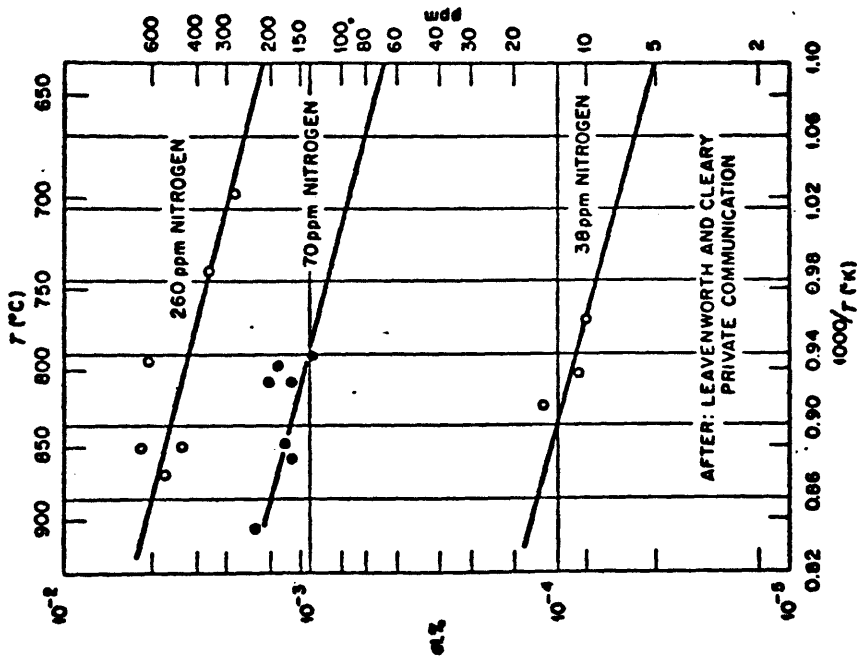


Figure 5a. The solubility of Niobium as a function of the temperature and the nitrogen concentration of liquid lithium.

TABLE 3

Test No.	Temperature		Lithium Nitride Addition to Lithium Weight Per Cent	Weight Change mg/in. ²	Metallographic Observations
	°F	°C			
1	1500	816	0.5	+ 2.4	8 mils of intergranular attack.
2	1500	816	1.0	- 12.3	35-mil tube wall completely penetrated intergranularly.
3	1500	816	2.0	- 1.0	35-mil tube wall completely penetrated intergranularly.
4	1600	871	0.1	0	35-mil tube wall completely penetrated intergranularly.
5	1600	871	0.25	- 4.0	35-mil tube wall completely penetrated intergranularly.
6	1600	871	1.0	- 14.8	35-mil tube wall completely penetrated intergranularly.

^aLithium nitride analysis: 58.4 Li - 37.1 N₂ - 1.5 CO₃ (weight per cent).

^bNitrogen content of lithium prior to addition of lithium nitride: 0.05 weight per cent.

Table 3. The effect of additions of lithium nitride^a to lithium^b on the corrosion resistance of type 316 stainless steel. Data from Hoffman (38).

that the grain boundary penetration of both tantalum and niobium is the result of ternary oxide formation within the containment metal grain boundaries.

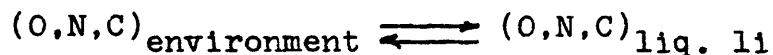
A spectrographic identification of ternary oxides has been achieved by Horsley⁽⁴⁵⁾ and verified by Hiltz⁽⁴²⁾ for the stainless steel-oxygen-liquid sodium system. The following reaction was reported by Horsley⁽⁴⁵⁾:



for the stainless steel-oxygen-liquid sodium system. Since the liquid sodium and liquid lithium reactions are very analogous, Hoffman⁽⁴⁶⁾ postulated that a Li_3NFeN complex compound would be present in stainless steel-nitrogen-liquid lithium systems.

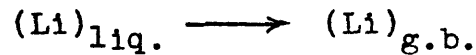
Complex compound formation has been shown to increase the grain boundary penetration and dissolution behaviors. Therefore, if the corrosion rate is to be perturbed, a better understanding of the mechanistic reaction steps is necessary. A possible representative series of reactions for the formation of the corrosion products could be the following:

Step 1. Solubility

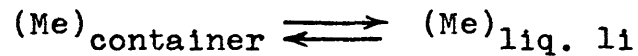


Step 2. Mass Transport

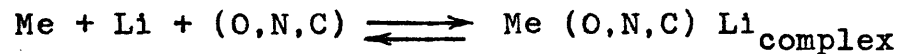
a. Grain Boundary Penetration



b. Dissolution



Step 3. Reaction (to lower free energy)



A possible perturbation to this set of reactions could be the removal of the impurity elements (O,N,C) from the liquid lithium and thus remove the formation of the complex compound.

Some investigations have been made^(13,46) on the removal of these active impurities by gettering. Gettering is the operation of alloying either the liquid lithium or containment metal with an element that has a lower free energy of formation of oxides, nitrides, or carbides than the lithium. Figure 6⁽²⁰⁾ shows a compilation of the free energies of formation for the important impurity species; oxygen, nitrogen, carbon. Hoffman⁽⁴⁶⁾ suggested that hot gettering liquid lithium with either titanium, zirconium or yttrium could reduce the corrosion rate of containment metals. Phillips⁽¹³⁾ used a yttrium hot trap to reduce the rate of corrosion in a liquid lithium-stainless steel convection loop. On the other hand,

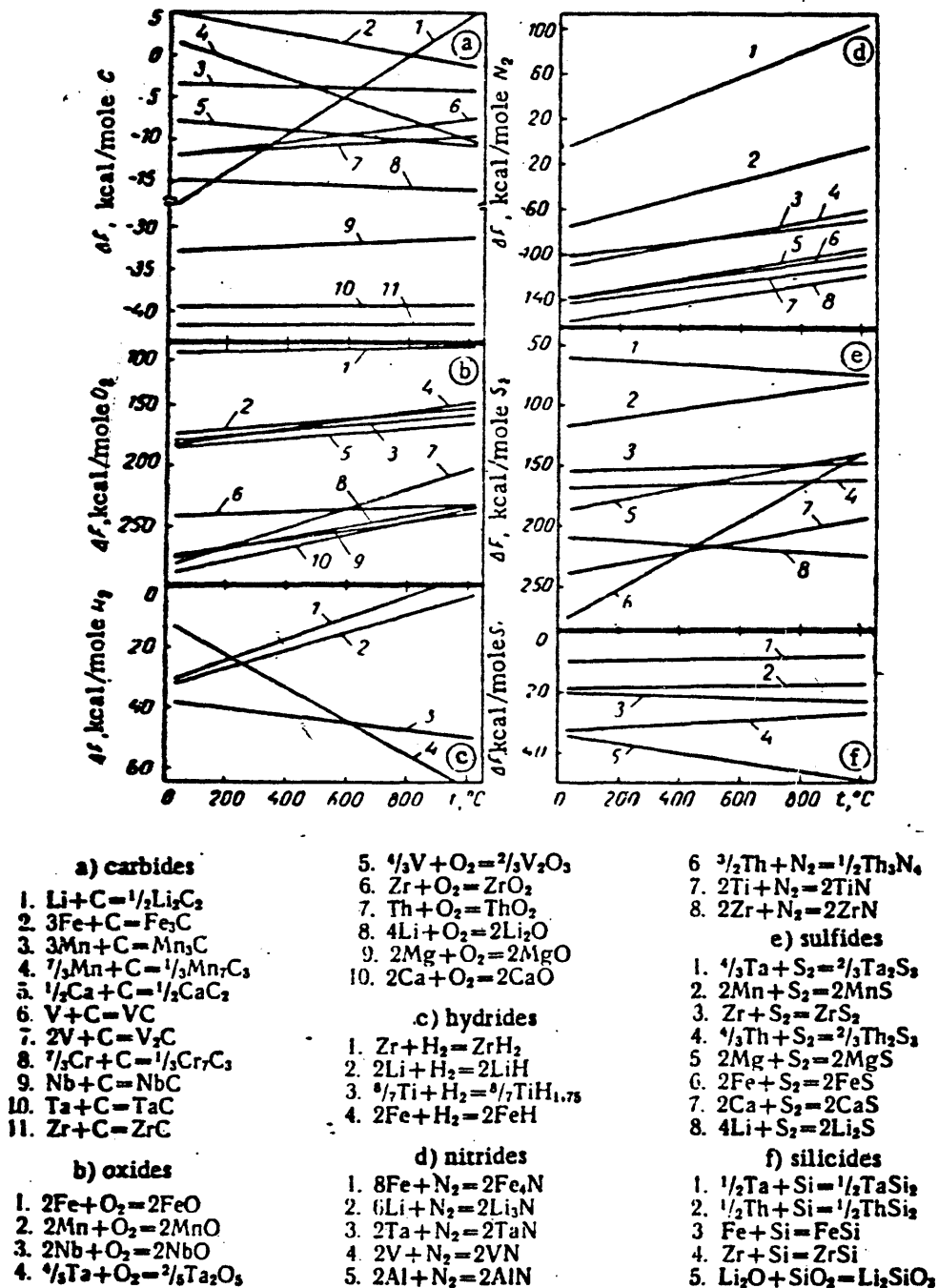


Figure 6. The temperature dependence of the free energies of formation of carbides, oxides, hydrides, nitrides, sulfides and silicides. Data from Popovich, et. al.(20).

Klueh⁽⁴⁰⁾ showed that alloy additions of less than 1 per cent Zr to Nb, stabilizes the oxygen concentration of the niobium and thus decreases the attack by liquid lithium. Therefore, the reduction of corrosion can be achieved by removing the complex compound forming impurities from the corrosion system.

Investigation

The corrosion system used in this investigation consisted of a stress-free sample, in contact with a static, isothermal liquid, and contained in a crucible that was chemically similar to the corrosion samples. Thus, the complex corrosion problem in liquid metal coolant systems was simplified to study the fundamentals of the 304L stainless steel-liquid lithium system. The experimental procedure and analysis of the data, with respect to the corrosion rate, are presented in the following sections.

EXPERIMENTAL PROCEDURE

Materials

Lithium used in this investigation was purchased from Research Organic Inorganic Chemical Corporation in the form of 99.9% pure - .635 cm - diameter rods. To assure safety and purity, the lithium was shipped submerged in mineral oil within sealed stainless steel containers.

The stainless steel specimens were type 304L received from the Republic Steel Research Laboratory.⁽⁴⁶⁾ Stainless steel 304L was also used to make the test crucible to eliminate dissimilar metal effects. The chemical analysis of the type 304L stainless steel used to construct the crucible is shown in Table 4.

All tests were conducted within a stainless steel glove box maintained at a positive pressure differential of .4 in. of water with 99.98% pure argon. Further atmospheric purification was accomplished by bubbling the incoming argon through a liquid sodium-potassium alloy and then maintained by stirring another flask of liquid sodium-potassium open to the glove box atmosphere at room temperature. Thus, when the surface of the liquid sodium-potassium was free of oxide, it indicated that low levels of oxygen contamination in the liquid lithium was present for each test. On the other hand, nitrogen saturation of the liquid lithium was assumed due to a solid lithium.

TABLE 4

Chemical Analysis
304L Stainless Steel

<u>Chemical Species</u>	<u>Weight Per Cent</u>
C	.026
Mn	1.60
P	.026
S	.030
Si	.49
Cr	18.48
Ni	9.16
Mo	.26
Co	.07
Cu	.17

nitride scale on the liquid lithium held in a stainless steel beaker at 300 C and also because each time the test crucible was opened, a solid lithium nitride scale was visible on the surface of the test lithium. This lithium nitride was not visible on tests above 800 C because above 800 C this species is not stable as can be seen from the Li_3N portion of the Li-N phase diagram in Figure 7.⁽⁵¹⁾

Apparatus

A schematic diagram of the test crucible and furnace arrangement is shown in Figure 8. Notable features of the crucible are that all sections in contact with the liquid lithium was made of 304L stainless steel to eliminate dissimilar metal effects, the crucible was sealed during each test by a press fit flange apparatus (but could be opened at time intervals to remove samples), and that as many as 20 samples could be suspended in the lithium without interactions between samples becoming evident. An auxiliary gas inlet and outlet system to allow the monitoring or variation of the test cover gas was also designed into the crucible. During this series of tests the argon present in the glove box was used as a cover gas.

All samples were suspended by pure iron wires which might have caused slight dissimilar metal effects, but since the wires did not show any evidence of preferential plating or corrosion upon removal, these effects were assumed to be negligible. Also the test region is held in approximately the

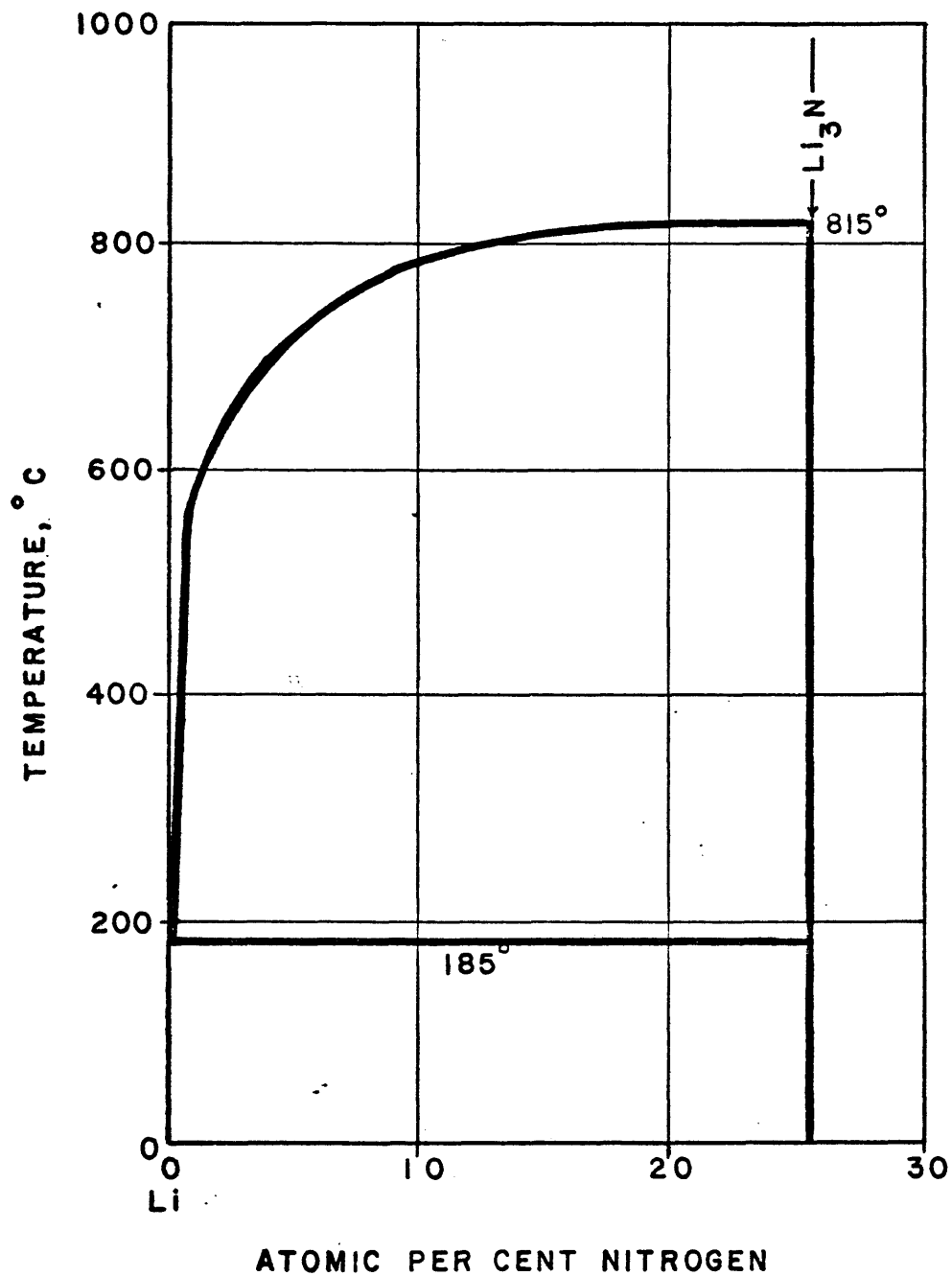


Figure 7. The Li_3N portion of the Li-N phase diagram after Elliot (50).

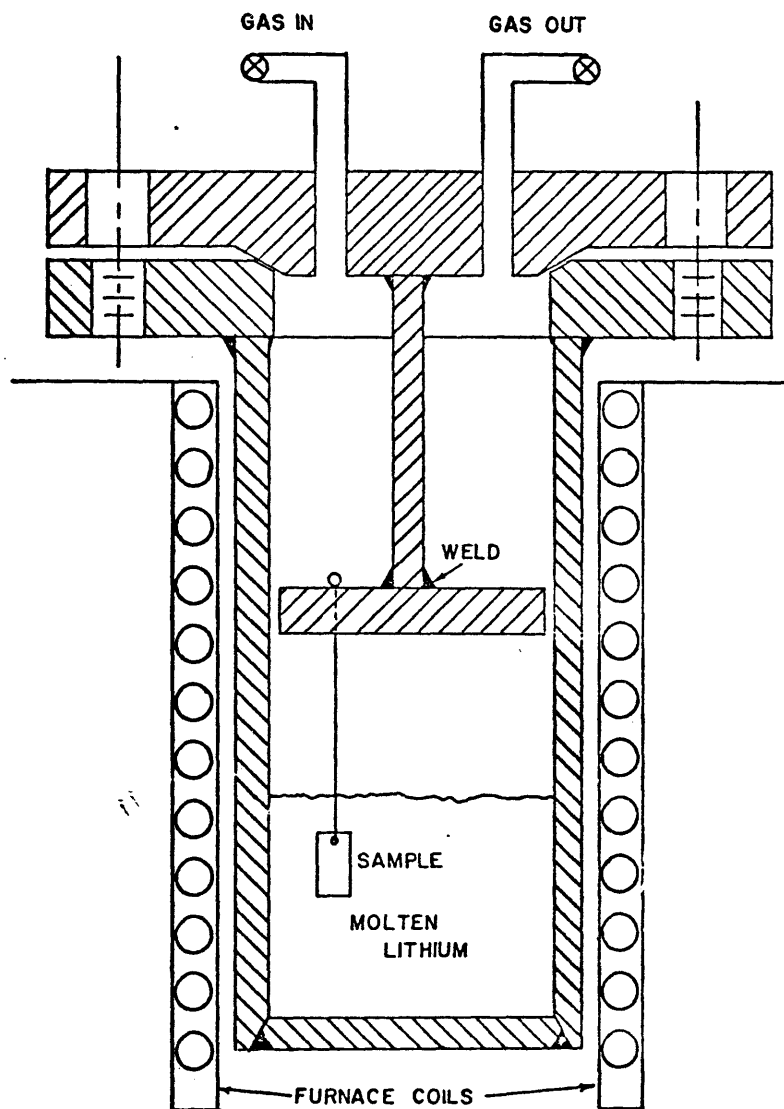


Figure 8. A schematic diagram of the test crucible and sample arrangement used in this investigation.

center of the heat zone of the furnace to eliminate temperature fluctuations. Temperature was held stable by the thermocouple sensor being fastened securely to the exterior of the test crucible with control maintained by a Marshall model 4044 proportional temperature controller accurate to ± 1 C.

Testing

The parameters being examined within the scope of this investigation are grain boundary penetration and weight loss as a function of time and temperature. Table 5 shows an outline of the test matrix used to determine these functional relationships.

Test specimens for the examinations were from a bulk sample of 304L stainless steel sheet. Each sample had the approximate dimensions and weight of .635 cm x 1.27 cm x .00762 cm and 0.5 grams. To remove the effects of prior work, homogenize the impurity concentration and obtain a uniform grain size, all samples were annealed at 900 C for 4 hrs. Following the anneal, all samples were polished on #1 grit silicon carbide paper to remove any surface oxide and then cleaned with methanol in an ultrasonic cleaner. Finally, before exposure, the samples were weighed on a Mettler H10 balance to $\pm .2$ mg, and thickness measurements were made with a micrometer, which had a maximum resolution of .0001 in. A typical micrograph of the 304L stainless steel following the heat treatment is shown in Figure 9. The samples were determined to have an average grain diameter of .0449 mm by the line intersection method. (56)

TABLE 5

Temperature C	600	650	727	800	900	1000
Penetration (max. time hrs.)	230	181	96	36	30	16
Weight loss (max. time hrs.)	420	445	400	180	107	--

Data generated by each of these tests is then summarized in Appendix I.

A matrix of the temperatures and times for each of the experiments performed in this investigation.

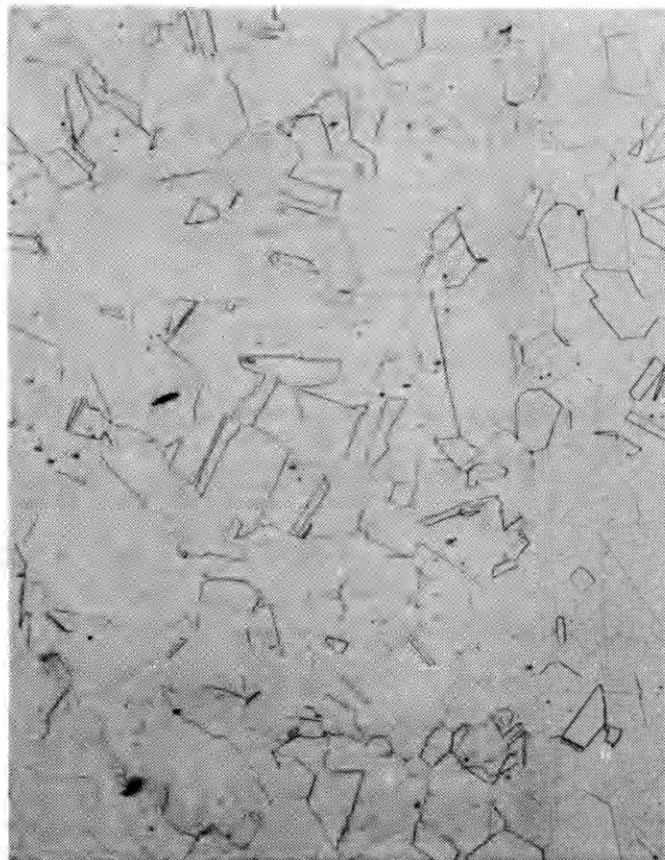


Figure 9. A micrograph of the 304L stainless steel after a four-hour heat treatment at 900 C. Magnification 200X.

The test procedure started with charging the crucible with 45 cm of .635 cm lithium rod which had been wiped clean to remove any surface compounds and mineral oil. Next the crucible was brought to the test temperature slowly and allowed to stabilize for at least 6 hours to achieve a quasi-equilibrium, with respect to the solubility, between the 304L stainless steel crucible and the lithium. This procedure was used to initiate a steady state dissolution-deposition reaction for each of the tests conducted. Leavenworth and Cleary⁽²⁶⁾ stated that 6 hours were sufficient to achieve equilibrium with respect to a dissolution reaction in liquid lithium. Following this stabilizing period, 304L stainless steel samples were introduced into the system to begin the test. During the test, sets of at least two samples were removed from the test apparatus at varying times. All samples were then submerged in water to remove any lithium surface coating and then subjected to a final ultrasonic cleaning in methanol. Analysis consisting of final weight measurements and metallography was then performed on these samples to reveal the test results.

Metallography

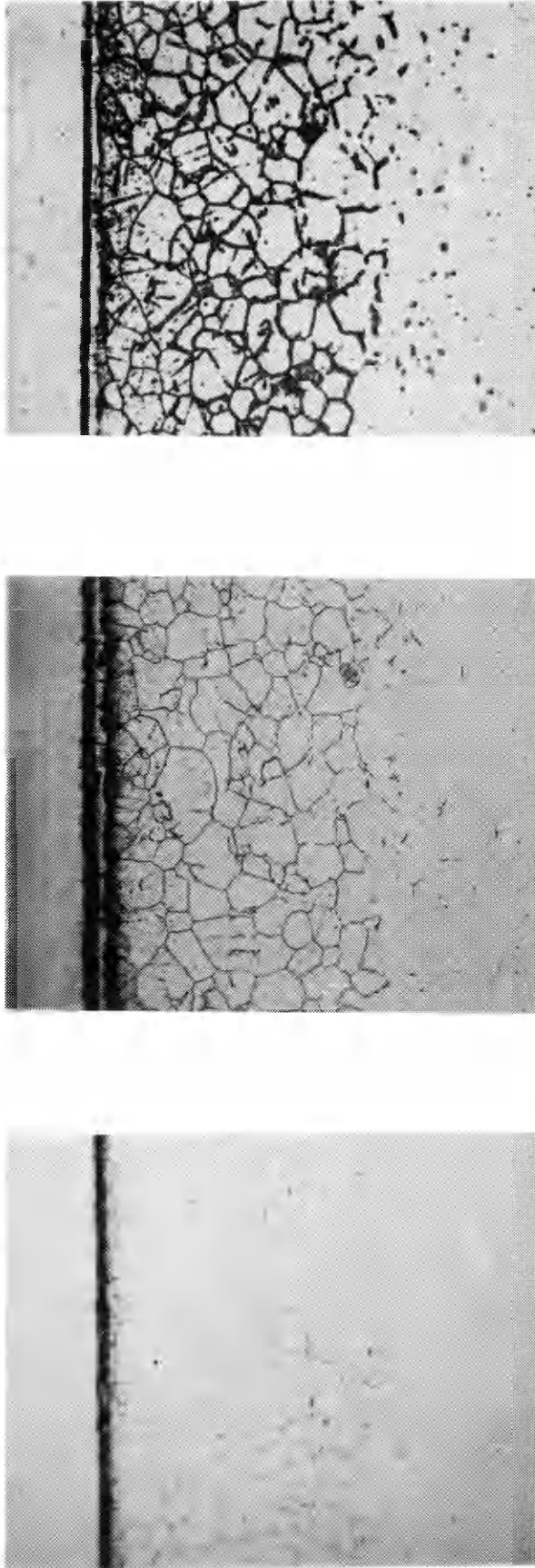
All grain boundary penetration measurements were done by a metallographic determination of the depth of corrosion products resulting from the migration of lithium into the stainless steel samples. Each sample was surrounded by metal straps protecting the edges from rounding or polishing damage and then mounted in Bakelite. The metallography consisted of

polishing each sample down to a .05 micron alumina wheel and followed by an etch in one of three equivalent etchant mediums. Three etches were investigated to eliminate the possibility that all penetration traces were not products of the etching technique. A list of these three etches is given in Table 6 along with etching parameters. Figure 10 shows that the three etches used give the same typical penetration pattern thus adding confidence to the metallographic procedure.

TABLE 6

<u>REAGENT</u>	<u>COMPOSITION</u>	<u>PROCEDURE</u>
FeCl_3 - HCl 1- used for most of the penetration study	FeCl_3 ----- 5 g. HCl -----50 ml H ₂ O-----100 ml	Etch for 60 seconds to reveal general structure plus penetration - follow by slight polish and etch for 20 seconds to reveal only the penetration.
Oxalic Acid	Oxalic Acid --- 10 g. H ₂ O ----- 100 ml	Used electrolytically with specimen as the anode. A current of .3 amps. for 2 minutes reveals the penetration very distinctly.
Chromic Acid	CrO ₃ ----- 10 g. H ₂ O----- 100 ml	Used electrolytically with specimen as the anode. A current of .8 amps for 15 seconds reveals the general penetration. Should also show any carbide precipitation.

A listing of the etches and metallography procedures used in this investigation.



a.

b.

c.

Figure 10. Typical micrograph showing the penetration zone as revealed by the a. FeCl_3 , b. Chromic Acid, c. Oxalic Acid, etches. The sample shown is number 5 from the 727 C C experiment. Magnification 220X.

RESULTS

The corrosion of container metals by liquid lithium has been related to two basic modes, preferential grain boundary penetration and surface deterioration (weight loss). The results of this investigation cite the data and analysis for static-isothermal-crucible tests using the 304L stainless steel-liquid lithium corrosion system. The grain boundary penetration depth as a function of time and temperature was obtained by a metallographic examination of the corroded 304L stainless steel samples, while the dissolution attack was studied by a measurement of weight loss per unit surface area as a function of time and temperature.

Brehm⁽³⁵⁾ related the penetration of niobium by liquid lithium to a diffusion controlled advance of a (Li-Nb-O) complex compound down the niobium grain boundaries. A dimensional analysis of this type of corrosion, which is based on a model assuming constant concentrations at the leading and trailing edge of the penetration, has been shown^(34,35,50,52, 54) to result in

$$x = \sqrt{kt} \quad (1)$$

where "x" is the depth of penetration as measured perpendicular to the liquid lithium containment metal interface and "k" is a temperature dependent constant. From Equation 1, "k" would

have the units of a diffusion coefficient, (cm^2/sec), and should follow the temperature dependence as defined by the Arrhenius relationship shown in Equation 2.

$$k = k_0 e^{-Q/RT} \quad (2)$$

In this equation, "Q" is the apparent activation energy for the penetration process.

The second mode of attack, dissolution in a static isothermal system, has been suggested^(10,39) to be controlled by the diffusion of alloying elements out of the containment metal to meet the requirements of chemical equilibrium as defined by the solubility of the alloying constituents in the liquid metal. Since the dissolution process for homogenous corrosion samples should be uniform over the entire surface area, the amount of weight loss per unit surface area is proportional to the thickness of the sample dissolved. Therefore, a similar relationship to that of Equation 1 will be used to characterize the weight loss-time dependence as shown in Equation 3,

$$\text{weight loss/unit surface area} = \sqrt{k't} \quad (3)$$

where "k'" is a new temperature dependent constant. However, the corrosion attack of containment metals has been shown⁽³⁷⁾ to be very non-uniform and thus the weight loss measurements are representative of a combination of both a uniform and localized attack.

The observations quoted in this section and in the review of the literature will be used to explain the experimental data and will allow a better understanding of the corrosion mechanisms.

Grain Boundary Penetration

All grain boundary penetration measurements were done by optical microscopy on samples prepared according to the methods mentioned in the metallography section. Depth of penetration measurements were made perpendicular to the sample edge with an average of at least 10 measurements for each sample. Figures 11 and 12 show plots of the depth of penetration versus the square root of time according to the parabolic nature of Equation 1. Figure 11 shows the temperatures of 600, 650, 727, 800 C and Figure 12 shows 800, 900, 1000 C. The rate coefficient "k" from Equation 1 was determined by a least squares analysis of all the data for each temperature in Figures 11 and 12.

Based on the response of the data illustrated in Figures 11 and 12, a hypothesis of a two step grain boundary penetration process was made. Intrinsic to this hypothesis was an initial temperature dependent delay time, which was followed by the parabolic penetration rate dependence. This recognizable delay time, when plotted versus temperature, reveals the C-shaped curve of Figure 13.

The shape of Figure 13 is very similar to that of the nucleation rate versus temperature curve shown in Brophy⁽⁵⁴⁾

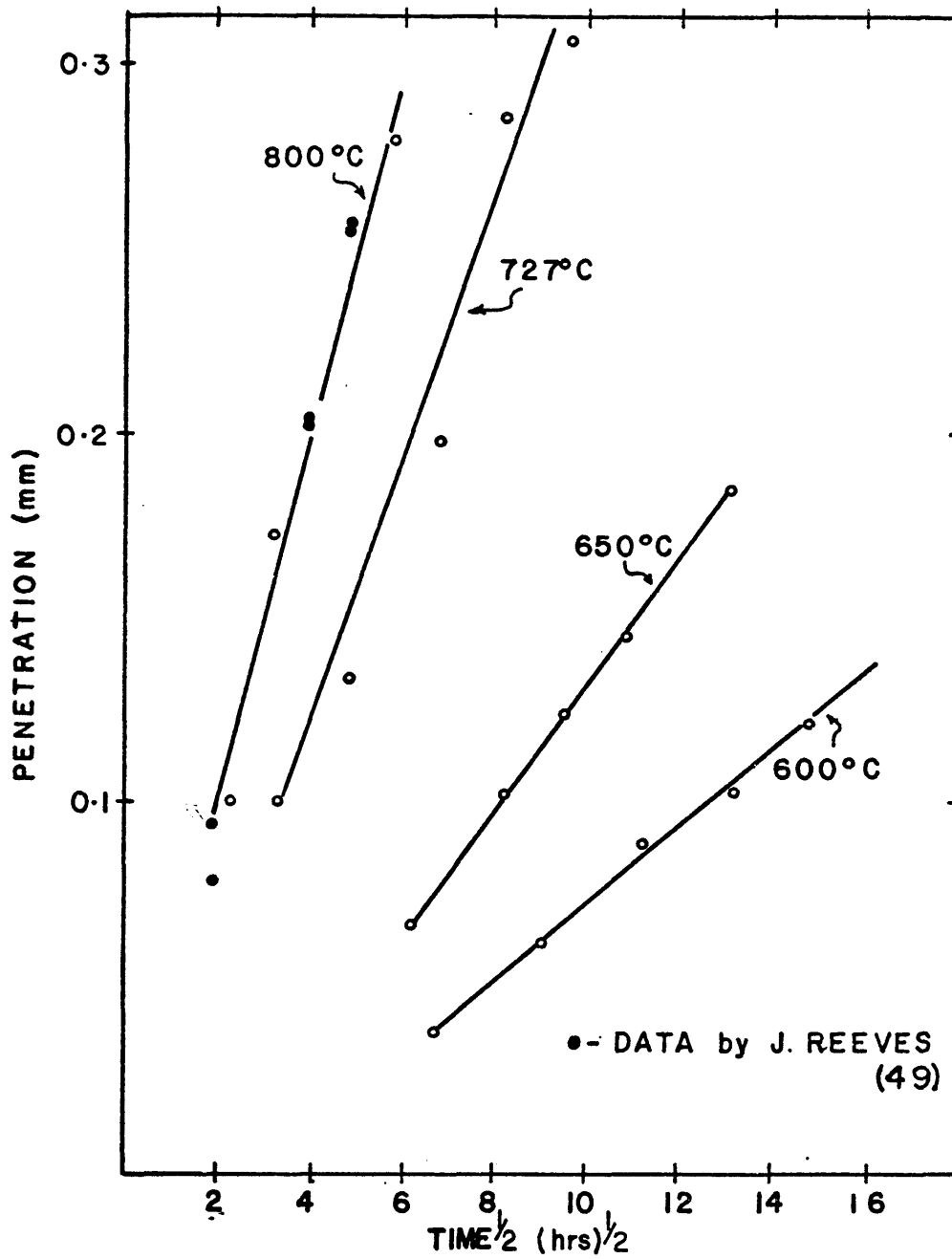


Figure 11. A graph of penetration depth versus the square root of time for the temperatures, 600, 650, 727, 800 C.

ARTHUR LAKES LIBRARY
COLORADO SCHOOL OF MINES
GOLDEN, COLORADO

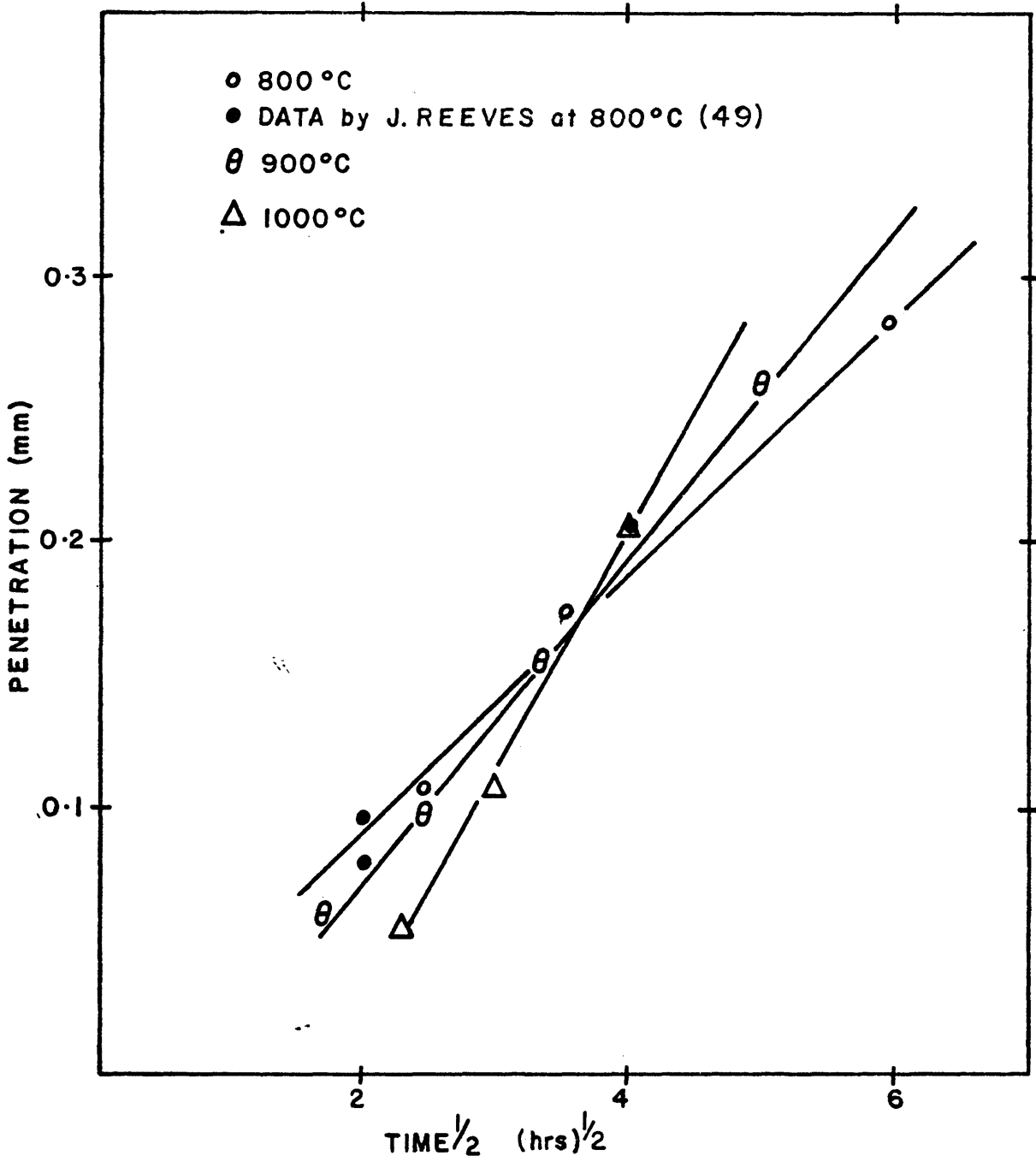


Figure 12. A graph of penetration depth versus the square root of time for the temperatures 800, 900, 1000 C.

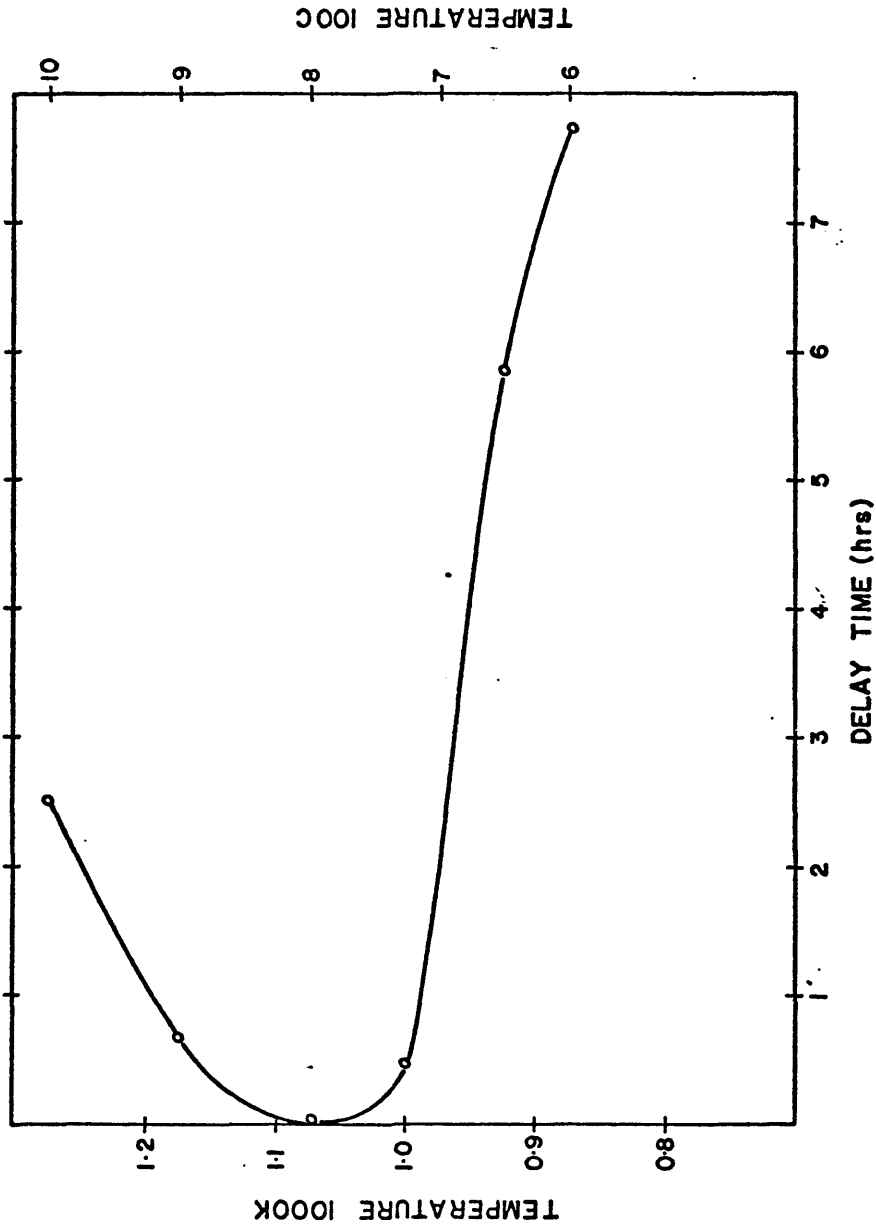


Figure 13. A graph of the temperature dependence of the observed delay time for the initiation of grain boundary penetration.

and Christian⁽⁵⁰⁾. Thus, if a (Li-Me-N) complex compound is assumed to be the corrosion product formed in the penetrated grain boundaries, the nucleation of this corrosion product could be the cause of the delay time.

Figure 14 shows the temperature dependence of "k" from Equation 1 as defined by Equation 2. The slope of the straight lines of Figure 14 relates to the apparent activation energies for the penetration process, "Q". The change in "Q" with increasing temperature suggests that two sequential processes are responsible for the grain boundary penetration kinetics and that the slower process is the one that controls the rate of penetration. The rate constants "k" for the penetration process are listed in Table 7 and the subsequent activation energies derived from the Arrhenius plot of these rate constants are tabulated in Table 8.

Titanium Gettering

A titanium gettering experiment was performed to further substantiate the role of nitrogen in the grain boundary penetration behavior. Suggestions have been made^(10,37,39) that lithium corrosion is related to the formation of complex compounds of the type (Li-Me-N). If the formation of these complexes does play an important role, the rate of penetration should decrease with the reduction of the concentration of nitrogen in the liquid lithium by the following reaction:



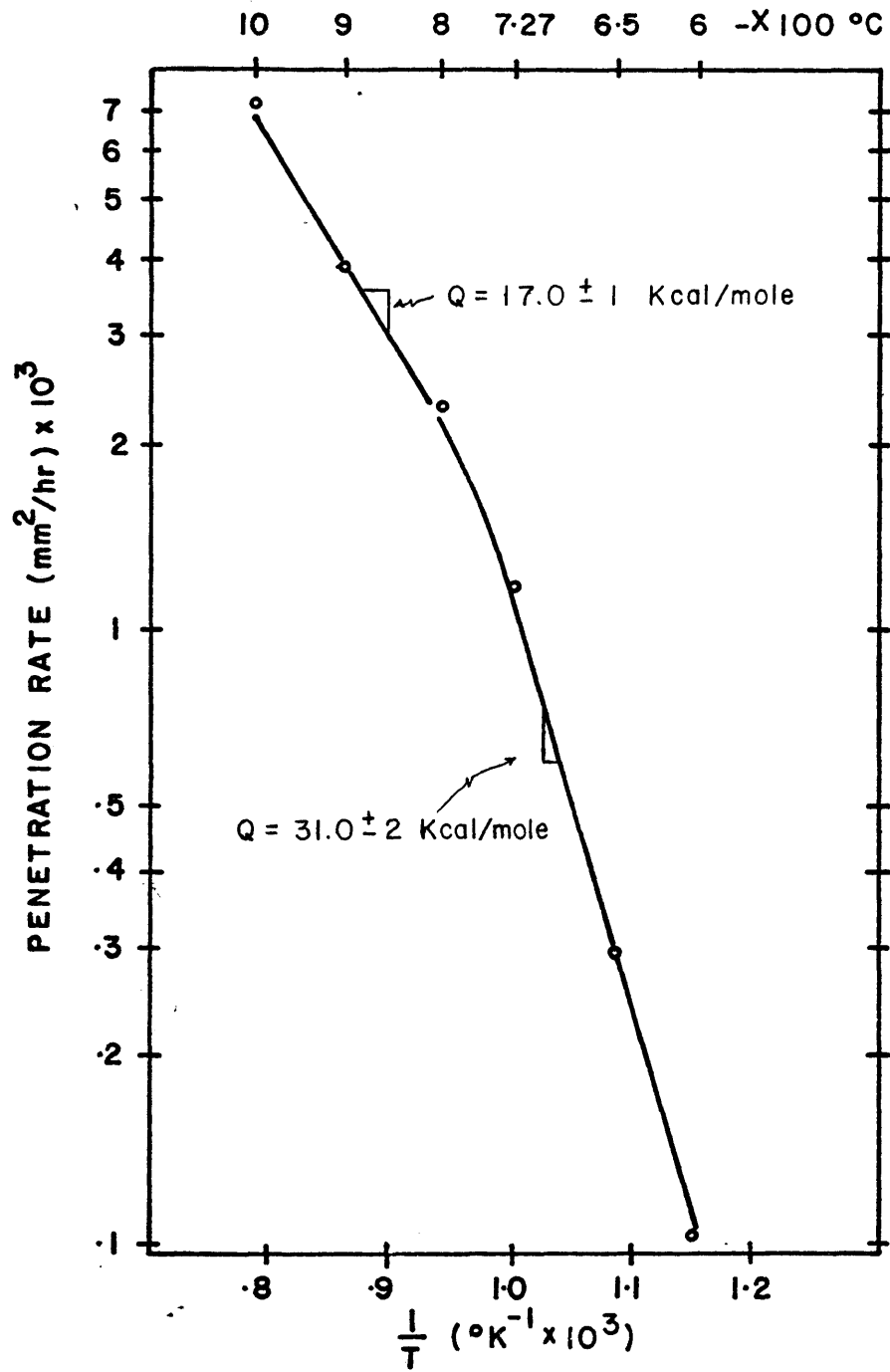


Figure 14. An Arrhenius plot showing the temperature dependence of the grain boundary penetration rate.

TABLE 7

Penetration Rate Constants

<u>T (°C)</u>	<u>T (°K)</u>	<u>1/T (°K⁻¹)</u>	<u>Rate k ($\frac{\text{mm}^2}{\text{hr}}$)</u>
600	873	.001145	.00010
650	923	.001083	.000296
727	1000	.0010	.001176
800	1073	.000932	.00228
900	1173	.000853	.00384
1000	1273	.000786	.00706

TABLE 8

Activation Energies

Below 800 C -----	31.0 ± 2.0 Kcal/mole
Above 800 C -----	17.0 ± 1.0 Kcal/mole

which goes to the right since TiN has a lower free energy of formation than Li_3N as illustrated in Figure 6.

Figure 15 shows a comparison of penetration depth versus the square-root of time for the nitrogen saturated lithium and the titanium gettered lithium tests at 800 C. The reduction in the grain boundary penetration rate suggests that nitrogen does indeed play an important role in the rate of grain boundary penetration.

With the nitrogen removed from the liquid lithium by gettering, the formation of the (Li-Me-N) complex must change or a new source of nitrogen must be found.

Reliability of Data

One of the major questions raised when evaluating the results of any experiment is the reproducibility of the data. Reeves⁽⁴⁹⁾ has reproduced the data quoted in this experiment by his grain boundary penetration data on 304L stainless steel in liquid lithium at 800 C, as shown in Figure 11. Also, the maximum error on the penetration data in this experiment was determined to be $\pm .005$ mm. Thus the reproducibility of the data seems to be within the limits of possible measurement error.

Dissolution and Surface Deterioration

Figures 16-20 illustrate the trends of the weight loss per unit surface area data for 304L stainless steel in liquid lithium. The linear nature of the weight loss data when

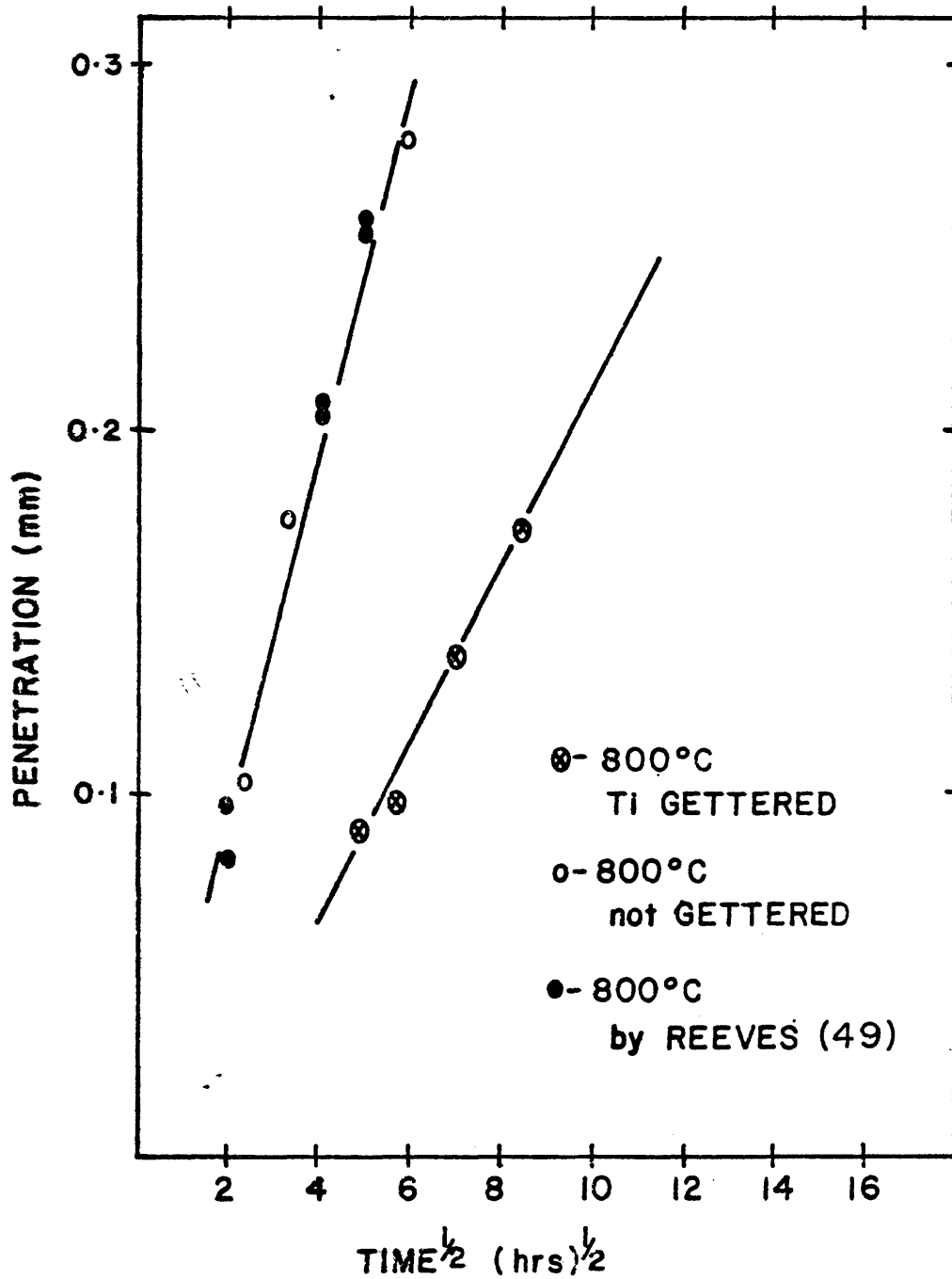


Figure 15. A plot of penetration depth versus the square root of time for the lithium at nitrogen saturation and for the titanium gettered lithium.

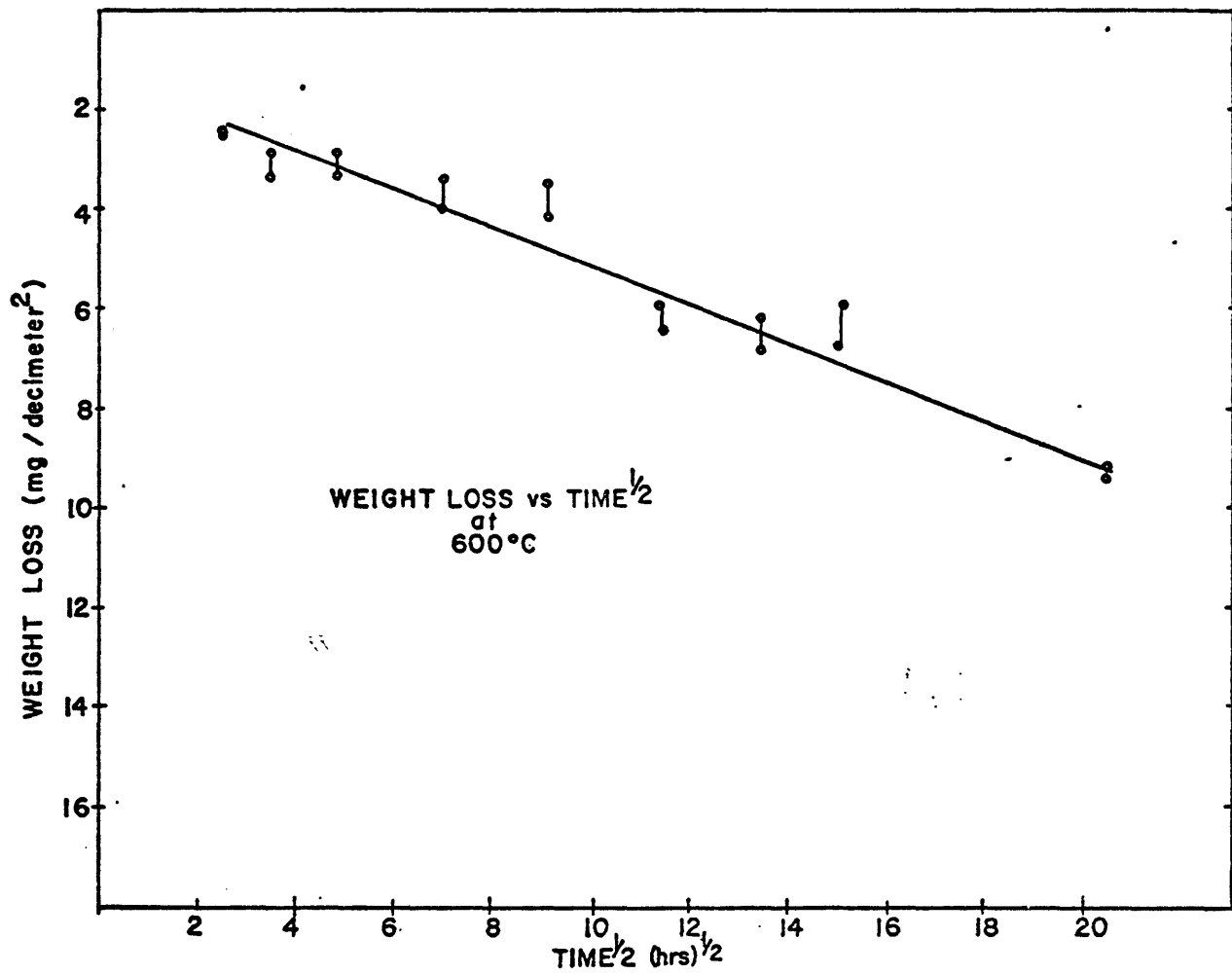


Figure 16. The plot of weight loss per unit surface area versus the square root of time for the experiment performed at 600 C.

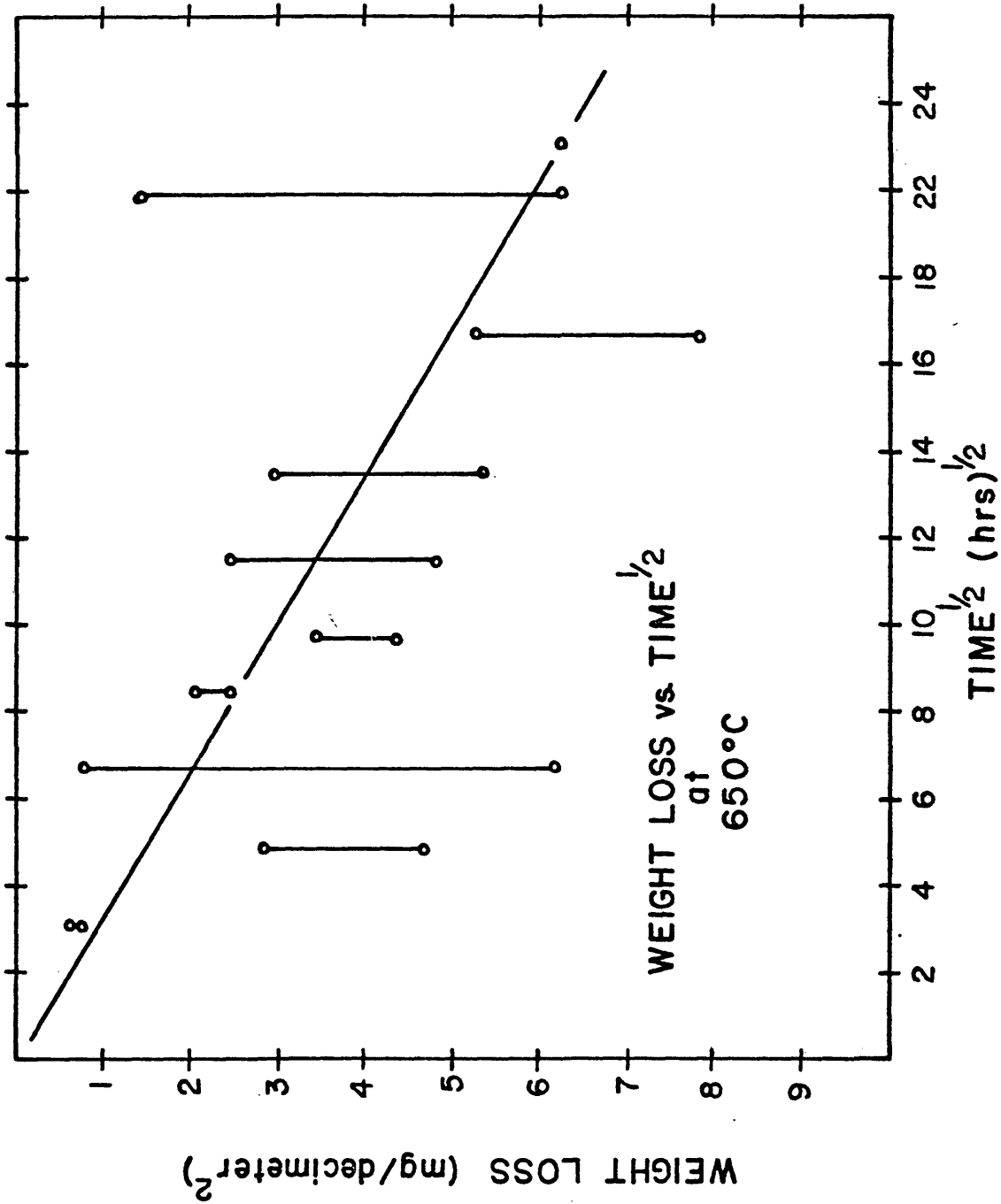


Figure 17. The plot of weight loss per unit surface area versus the square root of time for the experiment performed at 650 C.

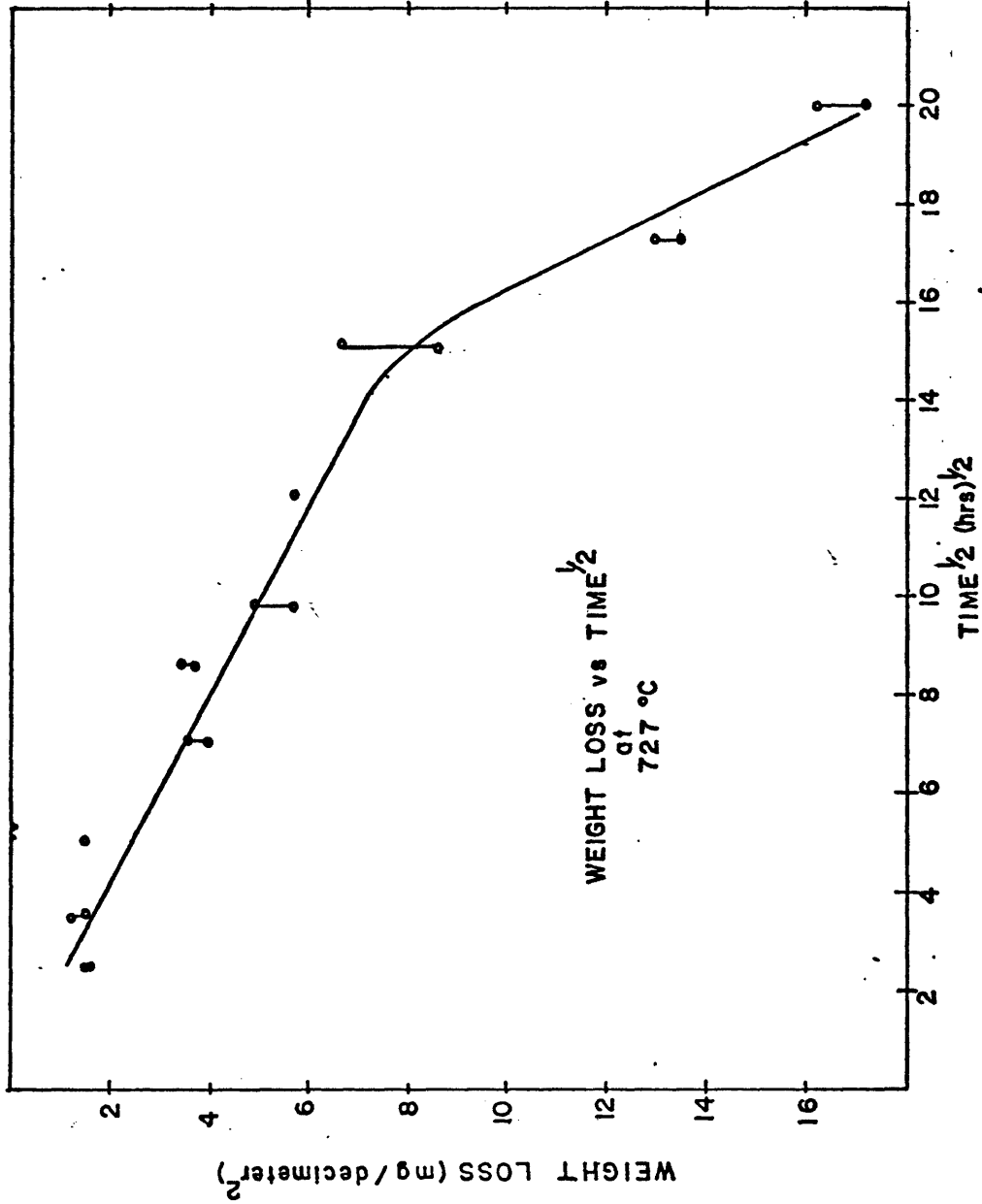


Figure 18. The plot of weight loss per unit surface area versus the square root of time for the experiment performed at 727 C.

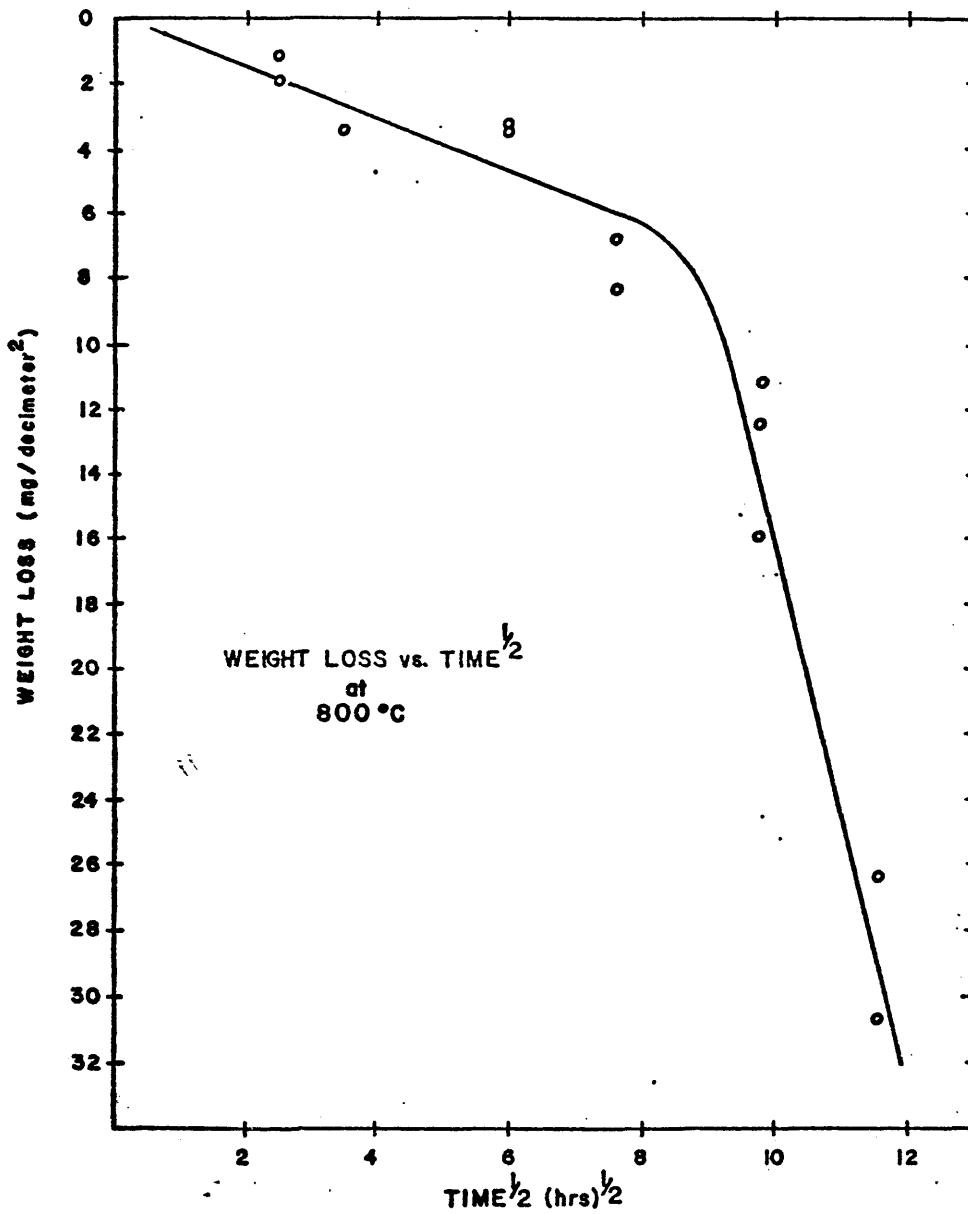


Figure 19. The plot of weight loss per unit surface area versus the square root of time for the experiment performed at 800 C.

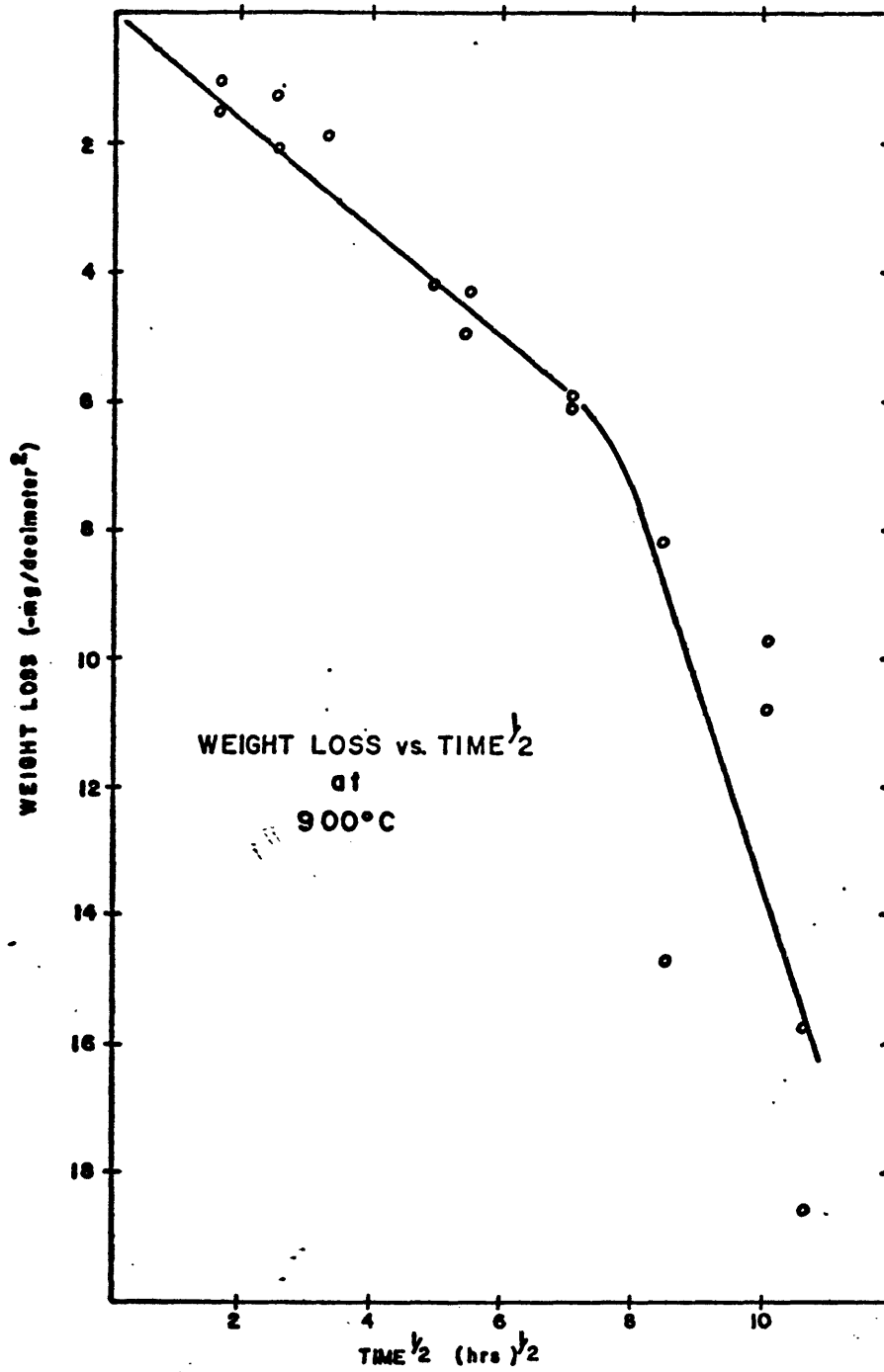


Figure 20. The plot of weight loss per unit surface area versus the square root of time for the experiment performed at 900 C.

plotted versus the square root of time, implies the presence of a uniform dissolution process as characterized by Equation 3. However, the change evidenced in Figures 18-20 indicates that a combination of corrosion mechanisms is present above 700 C. This duplex weight loss behavior was suggested by the author to be caused by the non-uniform nature of liquid lithium corrosion. Therefore the dissolution process, which has been defined in this thesis as a uniform mode of attack, is also coupled with a surface degradation or non-uniform mode of attack.

Disteffano and Hoffman⁽³⁷⁾ have identified an oriented transgranular penetration of containment metals by liquid lithium. Figure 10b shows that this transgranular penetration is also present in the liquid lithium penetration of 304L stainless steel. Since the non-uniform weight loss behavior was only predominant after the corrosion samples were completely penetrated, the non-uniform weight loss behavior is associated with the increased importance of surface degradation which may be caused by transgranular penetration.

An Arrhenius plot of the initial slope of the curves for 600, 727, 800, and 900 C is shown in Figure 21. This curve suggests that a thermally activated process is evident below 800 C for the initial weight loss behavior. The temperature at which the slope of this Arrhenius plot changes is consistent with the change observed in the grain boundary penetration behavior (Figure 13 and 14). This consistent behavior implies

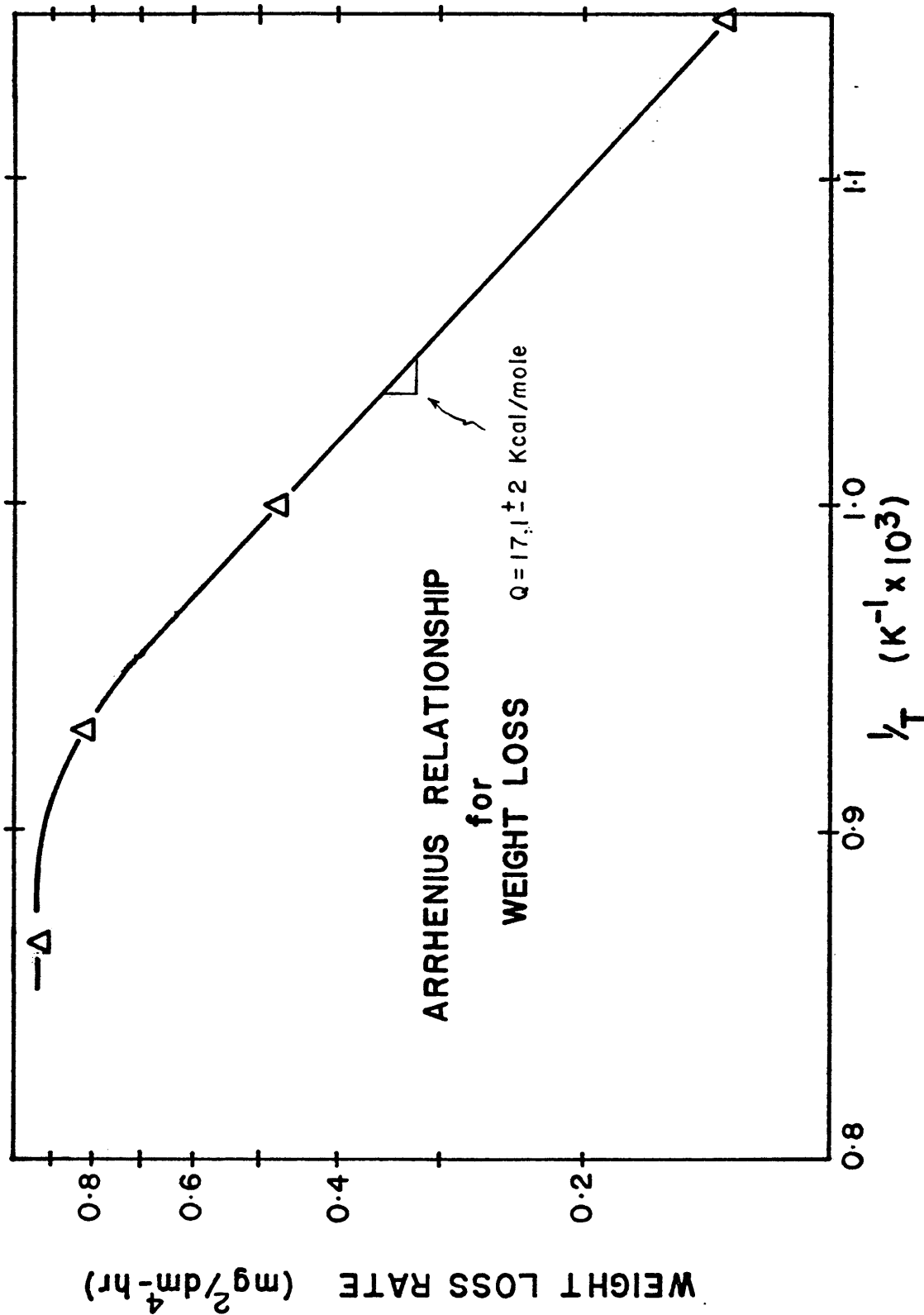


Figure 21. The possible temperature dependence of the initial slope of the weight loss curves. The experiment at 650 C is deleted due to the excessive scatter in data evidenced.

THUR LARKS LIBRARY
 COLORADO SCHOOL OF MINES
 GOLDEN, COLORADO

that similar mechanisms are evidenced for both the weight loss and grain boundary penetration investigations.

The weight loss rate coefficient for 650 C was not plotted on the Arrhenius plot of Figure 21, due to the excessive scatter in data for this temperature as shown in Figure 17. Also the values of the rate coefficients and activation energy for the weight loss data, as shown in Table 9, are not used to attempt a modelistic analysis due to the lack of sufficient data for any true statistical analysis.

Impurity Effects

Two investigations were performed to determine the effects of impurities on the weight loss behavior of 304L stainless steel in liquid lithium. These experiments consisted of two tests, one with titanium gettered liquid lithium and the other with nitric acid contaminated 304L stainless steel. The purpose of these two experiments was to see if perturbations of the test system would alter the form of the corrosion attack.

Titanium Gettering

Figure 22 shows the weight loss versus the square root of time curve for the titanium gettered lithium experiment at 800 C. A comparison of this curve with the nitrogen saturated liquid lithium weight loss curve of Figure 22 reveals that gettering the lithium reduces the amount of weight lost by the

TABLE 9

Weight Loss Rate Coefficients and Activation Energy

<u>T (°C)</u>	<u>T (°K)</u>	<u>1/T (°K⁻¹)</u>	<u>Rate Coefficient (mg²/dm⁴-hr)</u>
600	873	.001145	.1346
727	1000	.0010	.4896
800	1073	.000932	.8390
900	1173	.008525	.9137

Activation Energy Below 800 C-----17.1 ± 2 Kcal/mole

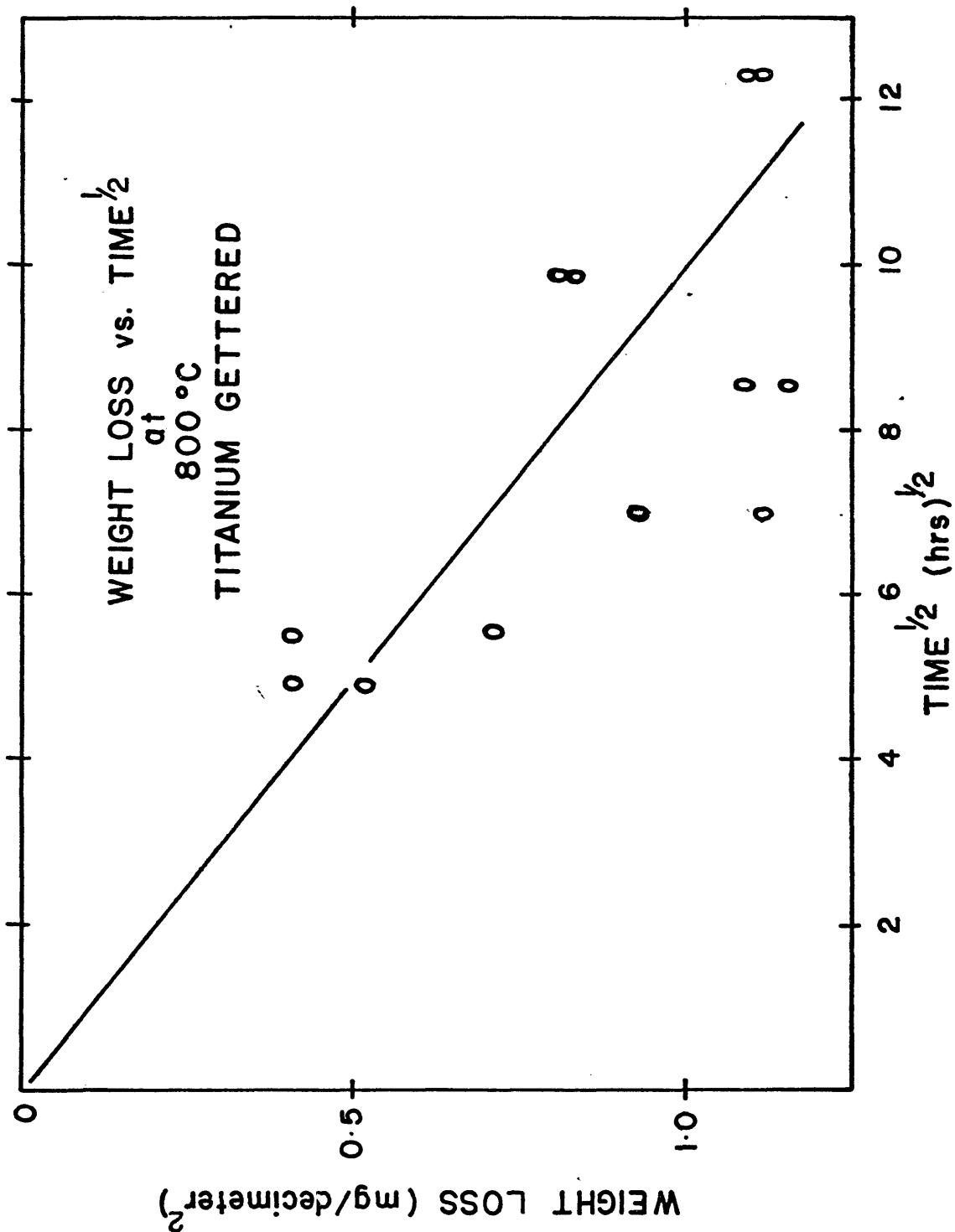


Figure 22. The graph of weight loss versus the square root of time for the titanium gettered experiment at 800 C.

304L stainless steel samples and eliminates the secondary non-uniform attack. This change in the severity of corrosion, with respect to weight loss measurements, is consistent with the reduction in grain boundary penetration rate for the titanium gettered system. This again infers that nitrogen plays an important role in the corrosion behavior of type 304L stainless steel in liquid lithium.

Nitric Acid Contamination

The corrosion behavior of the 304L stainless steel samples, when washed in nitric acid rather than methanol, reveals a completely different mode of attack. The micrograph of Figure 23 illustrates the uniform corrosion scale developed when the samples were washed in nitric acid prior to exposure to the liquid lithium. Some characteristics of this corrosion scale are that it emitted a strong ammonia smell when washed in water and that it was not strongly adherent to the uncorroded 304L stainless steel. An attempt to identify this corrosion product by X-Ray Diffraction was unsuccessful due to its amorphous nature. Horsley⁽⁴⁵⁾, however, was successful in identifying a similar scale in liquid sodium systems by spectrographic techniques, which revealed a (Na-Fe-O) complex compound.

Figure 24 illustrates the increased rate of weight loss behavior when the nitric acid contaminated 304L stainless steel samples are analyzed. This figure shows that the uniform

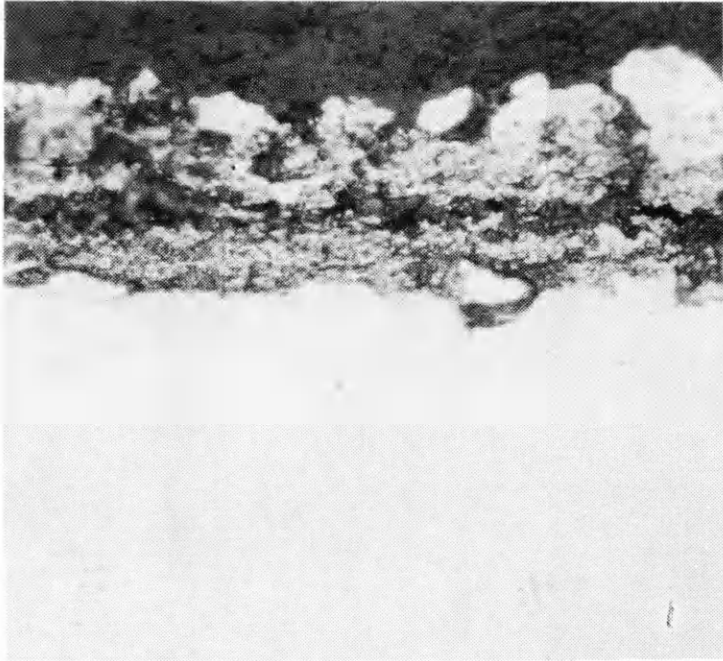


Figure 23. A typical micrograph of the uniform corrosion scale created when nitric acid contamination is present during the liquid lithium corrosion.

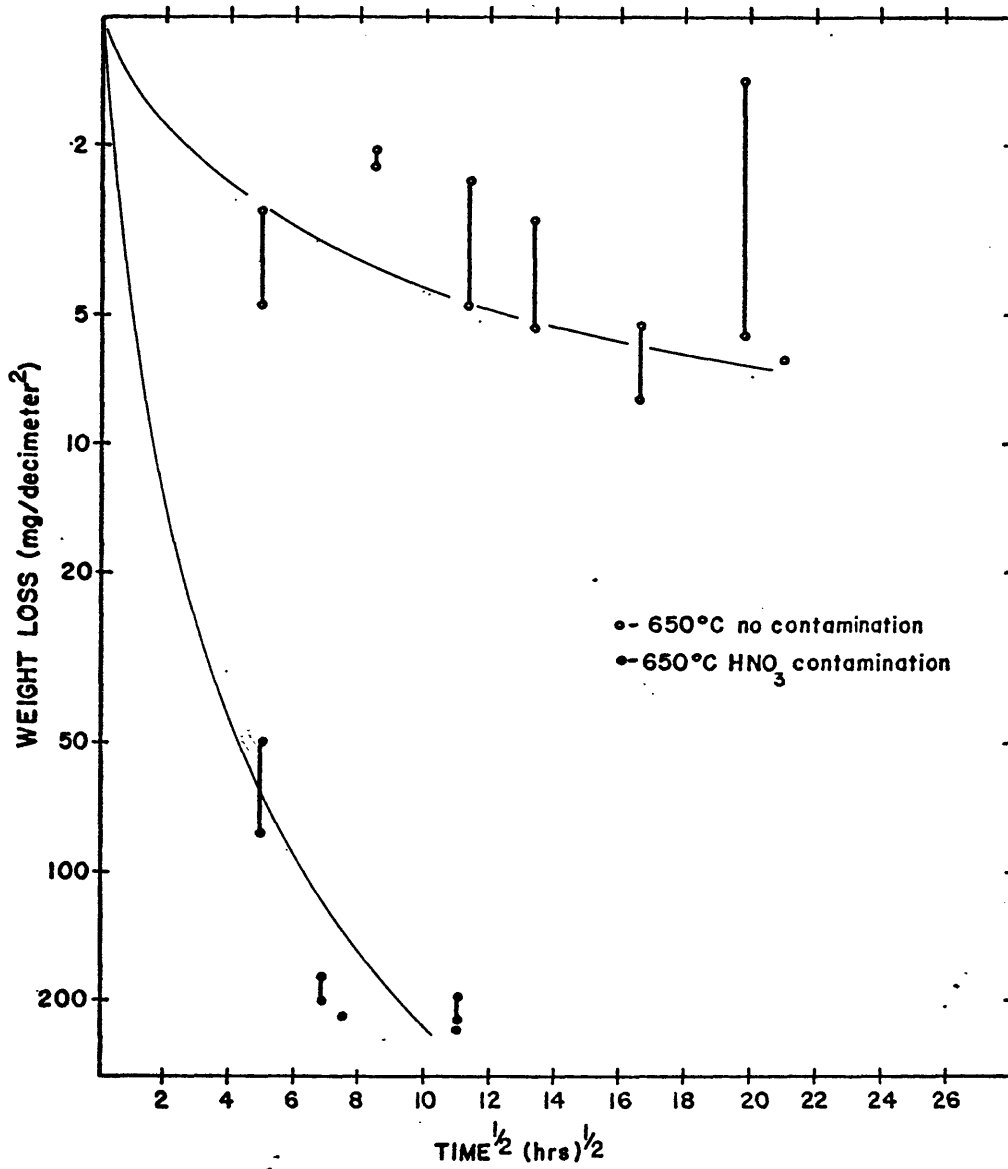


Figure 24. The comparison of the severity of weight loss between the methanol cleaned 304 L samples and the HNO₃ cleaned 304 L samples. The temperature of the test is 650 C.

corrosion caused by nitric acid contamination drastically changes the corrosion rate with respect to weight loss measurements.

The impurity effects mentioned draw important questions as to material handling procedures for nuclear coolant systems. This concern is primarily directed toward the cleaning techniques prior to service, especially with respect to cleaning with active reagents, i.e. nitric acid.

DISCUSSION OF RESULTS

The depth of grain boundary penetration was shown to be a parabolic function of time and dependent upon the nitrogen concentration of the liquid lithium. Also, a temperature dependent delay time was realized before the initiation of the penetration process. Rate coefficients and activation energies were reported and will be analyzed to understand the driving forces and controlling mechanisms responsible for the liquid lithium penetration into the type 304L stainless steel grain boundaries.

The assumptions that are necessary to define the mechanisms of the grain boundary penetration are listed below:

(1) The grain boundary penetration measurements are related to the preferential etching of a (Li-Me-N) complex compound, which is formed in the corroded 304L grain boundaries. The presence of this complex compound is consistent with the observations and assumptions of many investigators⁽³⁵⁻⁴⁶⁾ who studied the effects of impurities on corrosion by liquid metals.

(2) The formation of the corrosion complex at the grain boundaries is due to a heterogenous nucleation.

(3) The grain boundary diffusion of lithium into type 304L stainless steel would have a higher activation energy than the grain boundary diffusion of nitrogen. This assumption is based on the effect of strain on the activation energy.⁽⁵⁵⁾

Lithium's atomic radius is 1.55 Angstroms, while nitrogen's atomic radius is only 0.92 Angstroms. (55)

Delay Time

The probability that the corrosion product will form after a certain length of time is related to a balance of the energetic desire for nucleating a new phase and the ability to transport the atomic species. The delay time as a function of temperature is related to the rate controlling mechanisms for the formation of the assumed (Li-Me-N) corrosion complex. Initially the delay time decreases with increasing temperature which would suggest a mass transport control due to the increase in transport kinetics with increasing temperature. The inversion to increasing delay time with increasing temperature, may be explained by the free energy of formation of the corrosion complex becoming less negative at higher temperatures. If the corrosion complex is of the $\text{Li}_3\text{N}\cdot\text{FeN}$ type as suggested by Hoffman⁽³⁹⁾, the stability of the Li_3N compound can be used as a qualitative measure of the phase stability of the complex compound. As shown in Figures 6 and 7, the free energy of formation, and thus the stability of the Li_3N compound, is approaching zero at 800 C which corresponds with the temperature of the delay time inversion as shown in Figure 13.

Grain Boundary Penetration

Since the grain boundary penetration data was shown to follow a parabolic time dependence in this investigation, the

rate controlling mechanism is related to the mass transport of elements from the liquid lithium into the austenite grain boundaries. The assumed formation of a (Li-Me-N) complex compound in the austenite grain boundaries defines the diffusing elements to be either lithium or nitrogen. Therefore the activation energies reported for the grain boundary penetration study relate to the mass transport of either lithium or nitrogen through the two phase region, (Li-Me-N) complex-austenite, to a reaction interface.

The controlling atomistic process for grain boundary penetration changes at approximately 800 C, as is shown by the change in slope of the Arrhenius plot of Figure 14. This change implies that two sequential processes are taking place and that at 800 C a change in the rate controlling step occurs. Below 800 C, the activation energy was found to be 31.0 Kcal/mole. This is associated with the mass transport of lithium through the two-phase region, corrosion complex-austenite, due to the assumption that lithium should have a higher activation energy for diffusion than nitrogen. Above 800 C, the rate controlling step should be the diffusion of nitrogen through the two-phase region, to the reaction interface with an activation energy of 17 Kcal/mole. An illustration of these two sequential processes is shown in the Arrhenius plot of Figure 25. Substantiation for the shape of Figure 25 comes from the work by Reeves⁽⁴⁹⁾, who has found that the activation energy below 800 C is not altered when

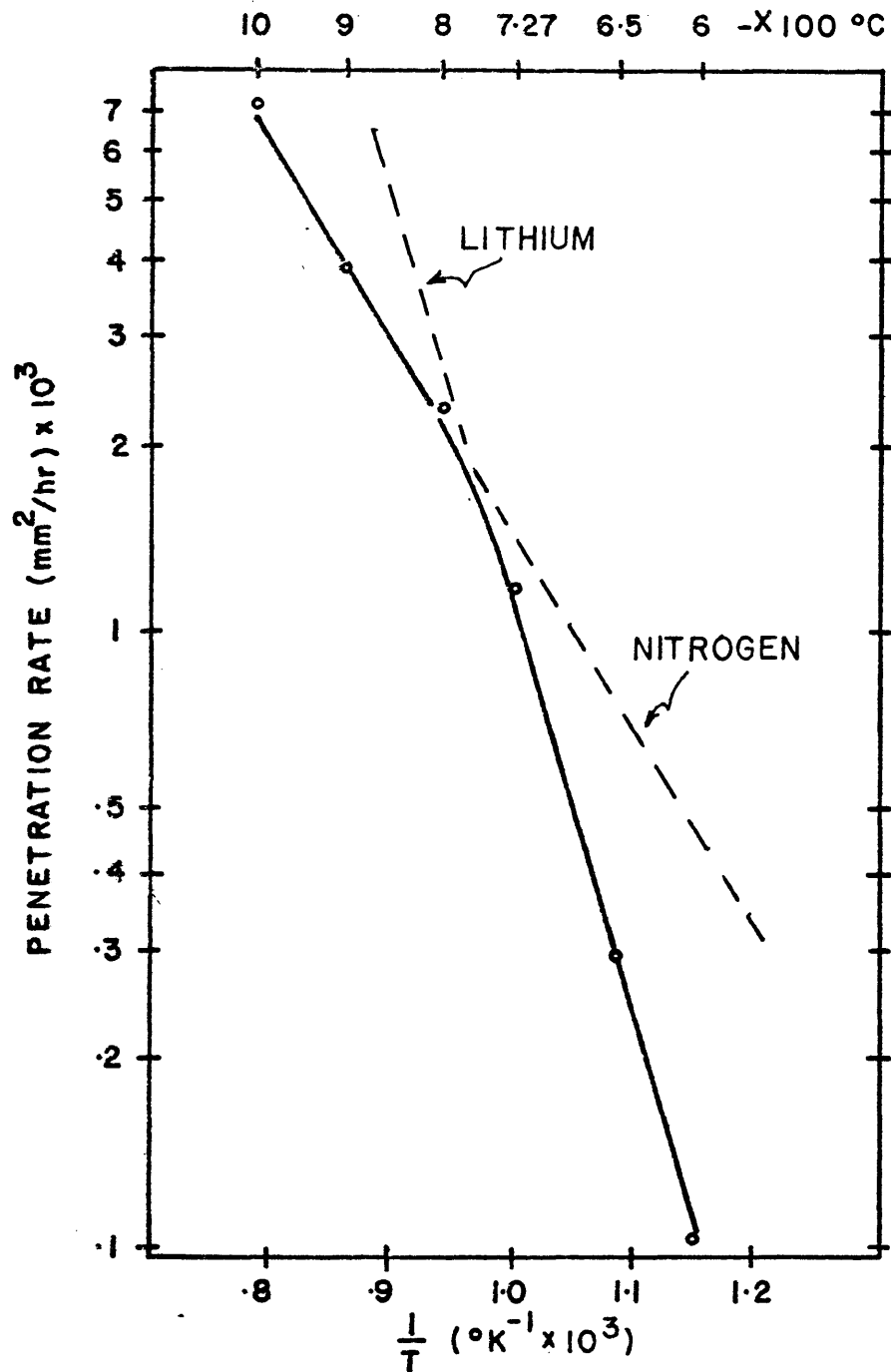


Figure 25. The proposed extension of each of the different activation energies. The solid line shows that the slowest moving species controls the rate of the reaction.

nitrogen saturated-304L stainless steel samples are exposed to liquid lithium. This implies that the transport of nitrogen does not control the penetration process below 800 C and therefore lithium control is postulated.

Since the concentration gradient of the diffusant is the driving force for the mass transport, the concentration as a function of time and distance from the sample surface allows a mathematical solution to this type of diffusion problem. Such a solution has been introduced by Wagner⁽⁵²⁾ and used by Brehm⁽³⁵⁾ to represent the diffusion into a homogeneous phase from the surface. Figure 26a illustrates this diffusion model, Region 1 corresponds to the two-phase region, (Li-Me-N) complex-austenite, and Region 2 is the homogeneous austenite phase.

Figure 26b illustrates the chemical potential gradient established by the diffusion. The chemical potential at the sample surface, μ_0 , is associated with the chemical potential of liquid lithium in its standard state and is constant for the duration of the grain boundary penetration. The chemical potential of the diffusant at the reaction interface, μ_1 , is also held constant and is defined by its solubility equilibrium between the complex compound and austenite grain boundaries. The mathematical relationship between these two chemical potentials would then be:

$$\mu_1 = \mu_0 + RT \ln a_d(x,t)$$

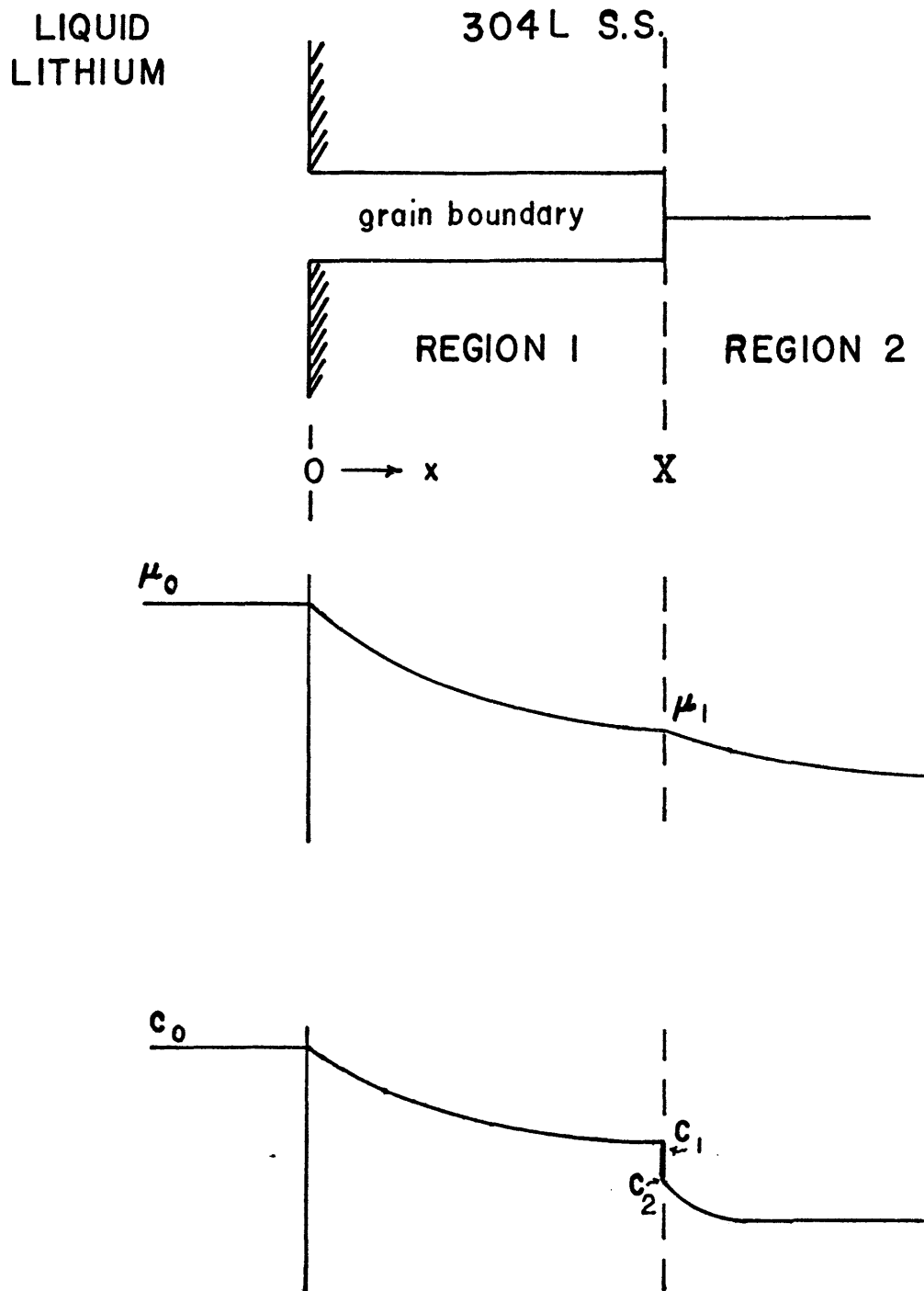


Figure 26. The schematic diagrams showing the regions defined by the diffusion model and the suggested chemical potential and concentration gradients inherent to these regions.

where $a_d(x,t)$ is the activity of the diffusant along the grain boundary as a function of distance, "x", from the surface and time. Assuming that the activity of the diffusant is directly proportional to its concentration according to Henry's law, the following relationship can be obtained:

$$(\mu_1 - \mu_0) = RT \ln C_d(x,t)$$

The differential equations which define the diffusion as it relates to these gradients in Regions 1 and 2 are shown below:

$$\frac{dc}{dt} = D_1 \frac{d^2c}{dx^2} \quad 0 < x < X$$

$$\frac{dc}{dt} = D_2 \frac{d^2c}{dx^2} \quad x > X$$

D_1 and D_2 are the diffusivities of lithium in Regions 1 and 2 respectively and are assumed to be independent of the concentration. The initial conditions relating to this system are:

$$c = c_0 \text{ at } x = 0 \quad t \geq 0$$

$$c = 0 \text{ at } x > 0 \quad t = 0$$

and the boundary conditions are:

$$c = c_1 \quad x = -X$$

$$c = c_2 \quad x = +X$$

Using these conditions a mass balance can be set up to show the amount of material needed to displace the boundary X by a displacement dX in the time dt is:

$$(c_1 - c_2) \frac{dX}{dt}$$

The diffusion relationship to achieve the displacement dX would then be:

$$(c_1 - c_2) \frac{dX}{dt} = -D_1 \left(\frac{dc}{dx} \right)_{-X} + D_2 \left(\frac{dc}{dx} \right)_{+X}$$

Solutions to these equations which are consistent with the boundary conditions are:

$$\text{Region 1 } c = c_o - A \operatorname{erf} \left(\frac{x}{2 \sqrt{D_1 t}} \right) \quad 0 < x < X$$

$$\text{Region 2 } c = c_o + B \left[1 - \operatorname{erf} \left(\frac{x}{2 \sqrt{D_2 t}} \right) \right] \quad x > X$$

where A and B are constants. The relationship for Region 2 assumes that there is some solubility of lithium ahead of the corrosion complex phase. The error function in each of these diffusion equations has the form of:

$$\operatorname{erf} z = \sqrt{\frac{4}{\pi}} \int_0^z e^{-s^2} ds$$

and the derivative is:

$$\frac{d \operatorname{erf}(z)}{dz} = \sqrt{\frac{4}{\pi}} e^{-z^2}$$

therefore the mass balance can be simplified to remove the partial derivatives as follows:

$$(c_1 - c_2) \frac{dX}{dt} = -A \sqrt{\frac{4}{\pi}} \frac{D_1}{\sqrt{4D_1 t}} \exp\left[\frac{-x^2}{4D_1 t}\right] + \sqrt{\frac{4}{\pi}} \frac{BD_2}{\sqrt{4D_2 t}} \exp\left[\frac{-x^2}{4D_2 t}\right]$$

From a dimensional consideration it can be shown that the following relationship must apply:

$$x = \sqrt{kt}$$

Thus, this analysis of the diffusion problem is consistent with the parabolic time dependence of the grain boundary penetration data. Although solutions to other diffusion equations will result in the same time dependence, this particular solution displays the best correlation with the physical corrosion behavior was observed in this thesis.

Impurity Effects

As can be seen from Figure 27, the concentration of nitrogen affects the rate of penetration. An increased rate is evidenced when the 304L stainless steel is doped to a saturation of nitrogen as is shown by Reeves⁽⁴⁹⁾ at 800 C and a decrease in rate is shown when the concentration of nitrogen in the lithium is decreased by titanium gettering at 800 C. However, Reeves⁽⁴⁹⁾ has observed that the activation energy for the grain boundary penetration process was the same for the experiments run in this investigation and his experiments using nitrogen saturated 304L stainless steel samples.

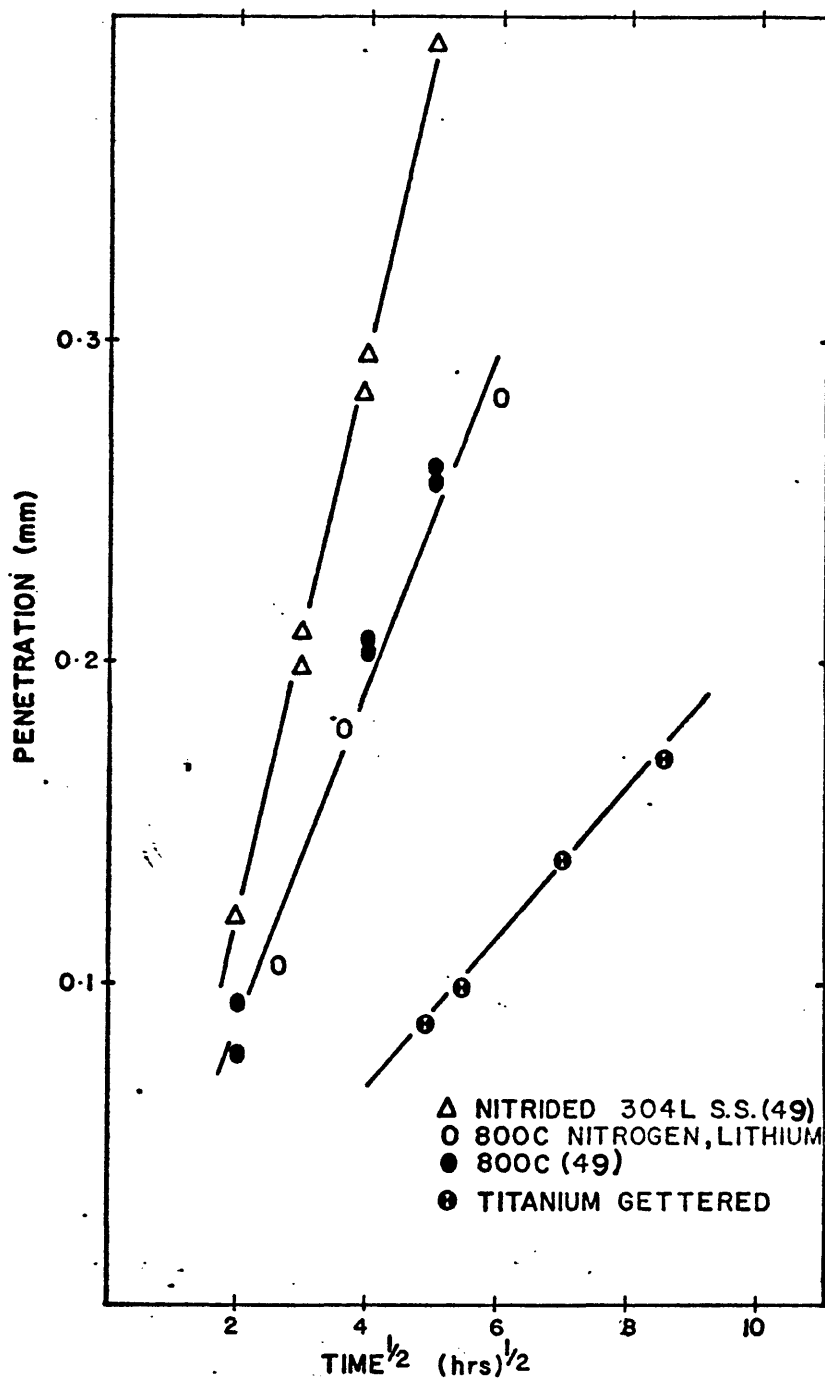


Figure 27. The penetration depth versus the square root of time for varying concentrations of nitrogen. The steepest sloped line corresponds to tests performed by Reeves (48) on 304 L stainless steel samples saturated with nitrogen. The intermediate sloped line corresponds to the nitrogen saturated lithium test and the shallowest sloped line is the titanium gettered lithium test.

Therefore, changes in nitrogen concentration must alter the pre-exponential coefficient of the Arrhenius relationship rather than the activation energy term.

The diffusivity of lithium into the grain boundary of the 304L stainless steel follows the normal temperature dependence as shown by the following equation and Figure 14:

$$D = D_0 \exp\left(\frac{-Q}{RT}\right)$$

in which Q is the activation energy relating to a probability for diffusion process and D_0 is the frequency factor. This D_0 is suggested to be dependent upon the impurity concentration influencing the diffusing atoms. Therefore if D_0 is a function of (O-N-C) impurities the rate of the equation would change but the dependence on temperature, Q , would remain constant. This change in D_0 is probably due to a stoichiometric change in the complex compound, which would affect the jump frequency, ν , and the entropy of mobility, ΔS , as seen in the definition of D_0 :

$$D_0 = \nu a^2 \exp\left(\frac{-\Delta S}{R}\right)$$

The large change found in this investigation with variation in nitrogen concentration is most likely an entropy contribution.

CONCLUSION

There are many interesting facets to this investigation- among the most important are the following:

(1) The mode of weight loss is due to a combined uniform and non-uniform mode of attack.

(2) A delay time is observed before the preferential grain boundary attack begins. This delay time was correlated with a nucleation type initiation of a (Li-Fe-N) corrosion complex.

(3) The grain boundary penetration was shown to follow a parabolic time dependence which was consistent with a diffusion model.

(4) Both the weight loss and grain boundary penetration were shown to be dependent upon the impurity concentration of the liquid lithium. The titanium gettering experiment in this investigation showed that the nitrogen impurity concentration plays an important role in the attack of liquid lithium on 304L stainless steel.

(5) The activation energy below 800 C was shown to be representative of lithium diffusion into the type 304L stainless steel grain boundaries.

SUGGESTIONS FOR FURTHER RESEARCH

The results of this investigation leave many questions unanswered in the area of liquid lithium corrosion. A few of the more relevant areas are summarized below:

(1) The need for a means of accurately measuring the concentration of (O-N-C) impurities in the liquid lithium is very important. If these concentrations were known, a better knowledge of their purpose in the corrosion process could be obtained, and possible lithium purification methods could be exacted.

(2) An investigation to positively identify the corrosion product in the grain boundaries is necessary to lend credence to any model of the corrosion mechanism. This aspect is also necessary if the development of an alloy which is resistant to lithium corrosion is to be developed.

(3) Another approach to the perturbation of the corrosion process is the delay time observed in this investigation. If an exact knowledge of the cause of this delay time were known, aspects of this phenomenon could be used to retard the grain boundary penetration process.

(4) The possibility of alloying the lithium to remove reactive species is another area of research that needs clarification. Hot traps which getter impurities from the liquid metal are now in use, but it is felt that an optimization of this process is necessary.

APPENDIX IExperimental Data

The experimental data quoted here is the data converted into the values plotted for the various curves in this investigation.

Grain Boundary Penetration Data

	<u>Time (hrs)</u>	<u>Penetration Depth (mm)</u>
600 C	48	.04
	84	.064
	132	.091
	180	.105
	230	.123
650 C	45	.0707
	72	.105
	96	.132
	133	.148
	181	.190
727 C	12	.100
	25	.148
	49	.199
	72	.287
	96	.308

	<u>Time (hrs)</u>	<u>Penetration Depth (mm)</u>
800 C	16	.104
	12	.177
	36	.28
900 C	3	.059
	6	.0963
	11	.155
	30	.289
1000 C	5	.056
	9	.112
	16	.204
<u>Titanium Gettered Lithium</u>		
800 C	24	.0884
	31	.0971
	49	.139
	73	.170

Weight Loss Data

	<u>Time (hrs)</u>	<u>Weight Loss (mg/decimeter²)</u>
600 c	6	2.439
		2.600
	12	3.401
		2.887
	24	3.403
		2.811
	48	3.439
		4.071
	84	3.295
		4.233
	132	5.968
		6.500
	180	6.108
		7.081
	230	5.971
		6.990
	420	9.232
		9.391

	<u>Time (hrs)</u>	<u>Weight Loss (mg/decimeter²)</u>
650 C	10	0.718
		0.640
	24	2.812
		4.624
	45	6.370
		0.776
	72	2.034
		2.420
	96	4.374
		3.475
	133	2.406
		4.851
	181	2.930
		5.315
277	5.529	
	7.846	
388	5.487	
	1.400	
445	6.235	

	<u>Time (hrs)</u>	<u>Weight Loss (mg/decimeter²)</u>
727 C	6	1.697
		1.474
	12	1.519
		1.129
	25	1.533
		1.460
	49	3.533
		4.036
	72	3.766
		3.336
	96	5.712
		4.899
	145	5.684
		5.688
	226	6.624
		8.63
	289	13.515
		12.914
	400	16.338
		17.214

	<u>Time (hrs)</u>	<u>Weight Loss (mg/decimeter²)</u>
800 C	6	1.726
		1.591
		1.186
		1.834
	12	3.352
	36	3.346
		3.257
		3.244
	60	8.247
		6.739
	96	12.302
		11.144
		15.829
	132	30.653
		26.838
900 C	3	1.464
		1.023
	6	1.220
		2.065
	11	1.805
		1.675
	24	4.074
		4.191
	30	4.227
		4.957
	50	6.083
		5.966
	72	8.183
		14.664
	102	9.642
10.762		
107	18.556	
	15.669	

REFERENCES

1. E. Berkley and G. A. Whitlow, "Microstructural and Compositional Changes in Sodium - Exposed Stainless Steel by Scanning Electron Microscope", Chemical Aspects of Corrosion and Mass Transfer in Liquid Sodium, AIME, (1971), Pp. 65-100.
2. W. F. Brehm, et. al., "Radioactive Material Transport in Flowing Sodium Systems", Corrosion by Liquid Metals, Plenum Press, New York, (1970), Pp. 97-113.
3. K. T. Claxton and J. G. Collier, "Mass Transport of Stainless Steel Corrosion Products in Flowing Liquid Sodium", Chemical Aspects of Corrosion and Mass Transport in Liquid Sodium, AIME, (1971), Pp. 101-129.
4. J. Hopenfeld, "Corrosion of Type 316 Stainless Steel with Surface Heat Flux in 1200 F Flowing Sodium", Corrosion by Liquid Metals, Plenum Press, New York, (1970), Pp. 33-40.
5. P. Roy, "The Evaluation of Particulates Deposited in Flowing Non-isothermal Sodium Systems", Corrosion by Liquid Metals, Plenum Press, New York, (1970), Pp. 1-20.
6. W. E. Ruther, et. al., "Evaluation of Materials - Compatibility Problems in the EBR-II Reactor", Corrosion by Liquid Metals, Plenum Press, New York, (1970), Pp. 81-96.
7. S. L. Schrock, et. al., "Sodium Corrosion of Westinghouse Liquid Metal Fast Breeder Reactor (LMFBR) Materials", Corrosion by Liquid Metals, Plenum Press, New York, (1970), Pp. 41-62.
8. J. R. Weeks and H. S. Isaacs, "Corrosion and Deposition of Steels and Nickel-Base Alloys in Liquid Sodium", Advances in Corrosion Science and Technology, V. 3, Plenum Press, (1973).
9. G. A. Whitlow, et. al., "Sodium Corrosion Behavior of Alloys for Fast Reactor Applications", Chemical Aspects of Corrosion and Mass Transfer in Liquid Sodium, AIME, (1971), Pp. 1-64.

10. J. R. Weeks and C. J. Klamut, "Liquid Metal Corrosion Mechanisms", Corrosion of Reactor Materials, V. 27, No. 1, Vienna, (1962).
11. H. U. Borgstedt, "Grain Boundary Grooving of Type 304 Stainless Steel and Armco Fe Due to Liquid Sodium Corrosion ", Corrosion, V. 27, Mar., 1974, Pp. 113-114.
12. A. B. Johnson Jr. and W. F. Vogelsang, "An Assesment of Corrosion Product Transfer Problem in a CTR", Transactions American Nuclear Society, V. 17, (Nov., 1973), p. 150.
13. W. M. Phillips, "Some Alkali Metal Corrosion Effects in a Rankine Cycle Test Loop", Corrosion by Liquid Metals, Plenum Press, New York, (1970), Pp. 197-216.
14. M. I. Chaevskii and V. V. Popovich, "Mechanisms of Corrosion Cracking Metals Deformed in Contact with Molten Lithium", Fiziko-Khimicheskaya Mekhanika Materialov, V. 6, No. 5, (1970), Pp. 106-108.
15. G. Devries, "The Corrosion of Metals by Molten Lithium", Corrosion by Liquid Metals, Plenum Press, New York, (1970), Pp. 251-270.
16. M. S. Goikhman, "Changes in the Microgeometry, Microhardness, and Structure of the Surface of Certain Alloys Under the Influence of Lithium", Fiziko-Khimicheskaya Mekhanika Materialov, V. 16, No. 3, (1970), Pp. 107-109.
17. M. S. Goikhman and M. I. Chaevskii, "Corrosion Resistance of Alloy EI-437B in Lithium", Fiziko-Khimicheskaya Mekhanika Materialov, V. 6, No. 5, (1970), Pp. 106-108.
18. R. N. Lyon (ed.), Liquid Metals Handbook 2nd Edition, USAEC and Department of the Navy, Report NAVEXOS-p-733 (rev.), 1952.
19. W. M. Mueller, et. al., Metal Hydrides, Academic Press, New York, (1968).
20. V. V. Popovich, et. al., "Corrosion Resistance of Armco Iron in Liquid Lithium", Fiziko-Khimicheskaya Mekhanika Materialov, V. 31, No. 1, (1967), Pp. 23-32.
21. Lithium Corporation of America, "Lithium Metal", LICOA Product Bulletin, OG, 110, New York.

22. Lithium Corporation of America, "Lithium Metal as a Heat Transfer Medium", LICOA Product Bulletin, New York.
23. N. E. Holden and W. F. Walker, "Chart of Nuclides", Educational Relations, General Electric Co., N. Y., 12345, (Oct., 1972).
24. W. H. Sullivan, "Trilinear Chart of Nuclides", Oak Ridge National Laboratories, U. S. Government Office Washington D. C., (Jan., 1957).
25. W. D. Wilkinson, and W. F. Murphy, Nuclear Reactor Metallurgy, D. Van Nostrand Co., Inc., (1958), Pp. 263-288.
26. H. W. Leavenworth and R. L. Cleary, ACTA Metallurgica, V. 9, (1961), P. 519.
27. A. S. Brasunas, "Liquid Metal Corrosion", Corrosion, V. 9, March, 1953, Pp. 78-84.
28. E. E. Hoffman, "Liquid Metal Corrosion", Corrosion Fundamentals, University of Tennessee Press, (1956), P. 78.
29. B. A. Nevzorov and O. V. Starkov, "Controlling Stage in the Transfer of Carbon in the System Carbon Steel/Liquid Sodium/Cr-Ni Steel", Fiziko-Kimicheskaya Mekhanika Materialov, V. 3, No. 3, (1967, Pp. 257-260.
30. A. J. Romano, et. al., "Interaction Effects Between Dissimilar Metals in High Velocity Sodium at Temperatures up to 760 C. I. Mass Transfer of Vanadium onto Type 321 Stainless Steel", Corrosion by Liquid Metals, Plenum Press, New York, (1970), Pp. 21-32.
31. K. Natesan and T. F. Kassner, "Thermodynamics of Carbon Transfer in Sodium Steel Systems", Chemical Aspects of Corrosion and Mass Transfer in Liquid Sodium, AIME, (1971), Pp. 130-156.
32. R. B. Snyder, K. Natesan, and T. F. Kassner, "The Kinetics of Carburization - Decarburization process of Austenitic Stainless Steels in Sodium", Journal of Nuclear Materials, V. 50, (1974), Pp. 259-274.
33. G. A. Whitlow, et. al., "The Effects of Exposure to Flowing Sodium on Vanadium Alloys in Stainless Steel Containment Systems", Corrosion by Liquid Metals, Plenum Press, New York, (1970), Pp. 115-136.

34. R. W. Harrison, "The Effects of Welding Atmosphere Purity on the Lithium Corrosion Resistance of Refractory Alloys", Corrosion by Liquid Metals, Plenum Press, New York, (1970), Pp. 151-176.
35. W. F. Brehm Jr., "Grain Boundary Penetration of Niobium by Lithium", PhD Thesis, NYO-3228-11, Report #735, Cornell University, (1967).
36. J. H. DeVan and R. L. Klueh, "The Effect of O₂ on the Corrosion of Vanadium and V-20% Ti by Liquid Lithium", Transactions of the American Nuclear Society, V. 17, Nov., 1973, P. 149.
37. J. R. Disteffano and E. E. Hoffman, "Relation Between O₂ Distribution and Corrosion of Refractory Metals in Lithium", Corrosion of Reactor Materials, V. 2, Vienna, (1962).
38. J. R. Disteffano and A. P. Litman, "Effects of Impurities in Some Refractory Metal-Alkali Metal Systems", 20th Annual Conference of the National Association of Corrosion Engineers, March 13, 1964.
39. E. E. Hoffman, "Corrosion of Metals by Lithium at Elevated Temperatures", ORNL 2924.
40. R. L. Klueh, "Penetration of Refractory Metals by Alkali Metals", Corrosion by Liquid Metals, Plenum Press, New York, (1970), Pp. 177-196.
41. R. W. Harrison, "Corrosion of Oxygen Contaminated Tantalum in NaK", Corrosion by Liquid Metals, Plenum Press, New York, (1970), Pp. 151-176.
42. R. H. Hiltz, "The Corrosion of Stainless Steel in Oxygen Contaminated Sodium at 1200 F and 1400 F", Corrosion by Liquid Metals, Plenum Press, New York, (1970), Pp. 63-80.
43. D. L. Smith and T. F. Kassner, "Application of Thermodynamic and Kinetic Parameters of the V-O-Na System to Sodium Corrosion of Vanadium-Base Alloys", Corrosion by Liquid Metals, Plenum Press, New York, (1970), Pp. 137-150.
44. P. C. S. Wu and P. Chiotti, "Reaction of Fe-Cr-Ni Alloys with Oxygen-Containing Sodium", Transactions of the American Society, V. 17, Nov., 1973.

45. G. W. Horsley, "Corrosion of Iron by Oxygen Contaminated Sodium", *Journal of the Iron and Steel Institute*, (Jan., 1956), Pp. 43-48.
46. E. E. Hoffman, "Symposium on Newer Metals", ASTM Special Technical Publication, V. 272, (1959), P. 195.
47. R. L. Klueh, "Oxygen Effects on the Corrosion of Niobium and Tantalum by Liquid Lithium", *Metallurgical Transactions*, V. 5, (April, 1974), Pp. 875-879.
48. R. Ault, Republic Steel Research Laboratory, personal communication.
49. J. A. Reeves, Colorado School of Mines, personal communication.
50. J. W. Christian, Theory of Transformations in Metal and Alloys, Pergamon Press, (1965), Pp. 369-375.
51. R. P. Elliot, Constitution of Binary Alloys First Supplement, McGraw Hill, New York, (1965), P. 582.
52. C. Wagner, in W. Jost, Diffusion, Academic Press Inc., New York, (1952), Pp. 69-75.
53. P. G. Shewmon, Transformations in Metals and Alloys, Pergamon Press, New York, (1965), Pp. 369-375.
54. J. H. Brophy, R. M. Rose, and J. Wulff, Thermodynamics of Structure, John Wiley & Sons, Inc., New York, (1964), Pp. 104-108.
55. P. G. Shewmon, Diffusion in Solids, McGraw Hill Book Co., New York, (1963), P. 98.
56. R. E. Reed-Hill, Physical Metallurgy Principles, Van Nostrand Reinhold Co., New York, (1964), P. 487.